High Power, Broadband, Linear, Solid State Amplifier

3rd Annual Report
under MURI Contract No.
N00014-96-1-1223

for the period
September 1, 1998 – August 31, 1999

Sponsored by:
Office of Naval Research
John Zolper, Monitor

Submitted by:

Lester F. Eastman, P.I.
Cornell University
School of Electrical Engineering
425 Phillips Hall
Ithaca, New York 14853-5401
Tel: (607)255-4369
Fax: (607)255-4742
e-mail: lfe@iiiv.tn.cornell.edu

September 1999

REPORT DOCUMENTATION PAGE	Form Approved OMB NO. 0704-0188

1. AGENCY USE ONLY (Leave Blank)	2. REPORT DATE	3. REPORT TYPE AND DATES COVERED
	9/1/98-8/31/99	**3rd Annual Report**

4. TITLE AND SUBTITLE	5. FUNDING NUMBERS
High Power, Broadband, Linear, Solid State Amplifier	**MURI N00014-96-1-1223**

6. AUTHOR(S) **L.F.Eastman, V. Tilak, K. Chu, O. Ambacher,N. Weimann, B. Green, K. Webb, B. Foutz, M. Shur, G. Augustine, J.A. Smart, J.R. Shealy, W. Schaff, T.Eustis, J. Silcox**

7. PERFORMING ORGANIZATION NAME(S) AND ADDRESS(ES)	8. PERFORMING ORGANIZATION REPORT NUMBER
Cornell University, School of Electrical Engineering 425 Phillips Hall, Ithaca, NY 14853-5401	**none**

9. SPONSORING / MONITORING AGENCY NAME(S) AND ADDRESS(ES)	10. SPONSORING / MONITORING AGENCY REPORT NUMBER
Office of Naval Research, Dr. John Zolper, Monitor, Room 607, 800 N. Quincy St. Arlington, VA 22217-5660	**none**

11. SUPPLEMENTARY NOTES

12 a. DISTRIBUTION / AVAILABILITY STATEMENT	12 b. DISTRIBUTION CODE
Generally available to the public Approved for public release; distribution unlimited.	

13. ABSTRACT (Maximum 200 words)

Large periphery AlGaN/GaN HEMT's gave normalized power > 2 W/mm, and > 4 W/mm on sapphire and SiC substrates, respectively. A new processing method, using photolithography for all steps except for the gate, is being developed to reduce cost and raise throughput and reproducibility. The properties of the two-dimensional electron gas in undoped HEMT structures are compared with theory and explained by a combination of spontaneous and piezoelectric polarization, and by interface roughness. Static induction transistor processing has been developed. Circuits for broad band amplifiers are simulated, and a dual-gate cascade power stage has experimentally yielded 8 db higher gain. A non-linear model for HEMT power devices has been successfully developed. Theoretical models for electron transport in high electric fields have been compared with measured frequency response. Initial measurements of $1/f$ noise are being made. OMVPE growth has been developed to reach ~ 1,600 cm^2/V-s electron mobility with ± 7% thickness variation. MBE growth has reached the same electron mobility with ± 3% thickness variation and is able to deposit a 25 Å GaN cap layer for chemical protection. Growth by OMVPE on SiC substrates is underway but requires further optimization to reduce deep donors in the AlGaN barrier.

14. SUBJECT TERMS **Microwave transistor, Gallium Nitride, MBE and OMVPE growth, power combining circuits**	15. NUMBER OF PAGES **42**
	16. PRICE CODE

17. SECURITY CLASSIFICATION OR REPORT	18. SECURITY CLASSIFICATION ON THIS PAGE	19. SECURITY CLASSIFICATION OF ABSTRACT	20. LIMITATION OF ABSTRACT
UNCLASSIFIED	**UNCLASSIFIED**	**UNCLASSIFIED**	**UL**

NSN 7540-01-280-5500 **Standard Form 298 (Rev.2-89)** Prescribed by ANSI Std. 239-18 298-102

TABLE OF CONTENTS

I. OVERVIEW – Lester F. Eastman

This MURI has been underway for three years, covering research on the use of III-Nitride materials, devices and integrated circuits for amplifying very high microwave power. Emphasis has been placed on High Electron Mobility Transistors (HEMT's), with a smaller effort on Static Induction Transistors (SIT's). We have pioneered in the use of undoped pseudomorphic AlGaN/GaN HEMT structures, where the strong spontaneous and piezoelectric polarization induce a large two-dimensional electron gas (2DEG) density near $1X10^{13}/cm^2$. These undoped HEMT's have orders of magnitude lower $1/f$ noise than the doped equivalent, and also allow better reproducibility of the 2DEG density. We obtain somewhat higher 2DEG density with SiC substrates than with sapphire substrates, most likely due to reduced dislocation density with the former, as a result of a better lattice match. Using 300 μm thick sapphire substrates, HEMT's with a single gate, center fed, yielded > 4 W/mm, while large periphery devices with a 50 μm pitch distance between parallel gates yielded > 2 W/mm. In both cases the limiting operating heat power causes 300°C channel temperature according to our simulations. In more limited experience with SiC substrates, > 4 W/mm were obtained on large periphery devices. Due to gate leakage, these latter HEMT's on SiC had a limit of 40 drain-source bias, a condition that can likely be solved by adjusting growth conditions. A theoretical study of gate leakage at pinch off up to 300°C channel temperature has shown only 10's nA/mm, but in some growth runs unintentional deep donors raise this value. A new process for fabrication of HEMT's, allowing all but the gate to be fabricated by photolithography, is being developed. It was necessary to avoid exposure of the AlGaN to KOH, present in the photo resist developer. KOH reduces the 2DEG density when it etches open regions around each dislocation in the AlGaN. The new process also includes a method to reduce current slump, also known as DC to RF dispersion. After earlier determination of the dependence of f_t and drain-source breakdown voltage on gate length, the Johnson limit of the product of power times the square of the operating frequency times the load impedance can be evaluated. The operating frequency is chosen to be a third of f_t in order to yield ~ 10 db gain. This Johnson figure of merit for AlGaN/GaN HEMT's is $1.8X10^{23}$ $WHz^2\Omega$. For SiC MESFET's it is $1.1X10^{23}$ $WHz^2\Omega$, and for GaAs MESFET's it is $2.8X10^{21}$ $WHz^2\Omega$. Initial measurements of $1/f$ noise at RPI show a substantial correlation with current slump for earlier devices. The difficult process of fabricating SIT's has been developed, but to date the required level of active layer doping, $2\text{-}4X10^{16}/cm^3$ has not been available. Undoped layers have $< 1X10^{16}/cm^3$ donors, while doped ones have $> 1X10^{17}/cm^3$ doping. It is planned to get layers with the required doping grown at Lincoln Laboratory by HVPE. The HEMT devices have been modeled for non-linearity, with good success in matching class A/B power saturation experiments. Using this model, broad band circuit configurations are being simulated to compare with experimental results. Non-uniformly distributed power amplifiers and Wilkinson combining amplifiers are being developed. In addition to the usual single transistor power cells for these circuits, cascode devices have been fabricated and tested. They yield 10 db additional gain and show promise of having simpler impedance matching possibilities. Fundamental theory of electron velocity vs. electric field using Monte Carlo calculations,

and low field electron mobility have been carried out. Using the equal areas rule to determine the value of average electron velocity, a comparison with the measured f_t has been made. Assuming that the electrons only have to transit the distance under the gate yields a more than 1.5:1 discrepancy between the theoretical values and those deduced from experiments. It is thus likely that the high field drift region extends well beyond the HEMT gate. Electron mobility is shown to have three important scattering mechanisms in addition to that associated with charged dislocations as analyzed by our MURI earlier. At the desired 2DEG density of $1X10^{13}/cm^2$, the theoretical electron Hall mobility value, excluding the dislocation effects, is ~ 1,800 cm^2/V-s. The undoped HEMT structures grown by us on sapphire by both OMVPE and MBE are ≤ 1,600 cm^2/V-s. On SiC the 2DEG density is higher, yielding somewhat lower electron mobility, as expected from the theory.The OMVPE reactor developed uses a single temperature (~ 1040°C), single pressure (~ 10% of atmospheric) and single flow, allowing scale up. Eight 2-inch wafers are grown during a run, and thickness uniformity is presently ~ ± 7%. This reactor has become attractive to industry, and two companies are negotiating licenses to use its patented design. The gas-source MBE uses nitrogen gas with an RF plasma to yield atomic nitrogen. Single-temperature growth is at ~ 800°C , and the thickness uniformity is presently ± 3%. All MBE growths of HEMT's have 25 Å GaN cap layers to reduce gate leakage by more than 10:1, and to chemically protect the structure from any accidental exposure to KOH during processing. In addition to OMVPE reactor design licensing, technology transfer of materials, processing methods, and devices are underway. Sanders, HRL, and GE have gotten materials, and devices have been tested by Sanders, Motorola, NRL, and AFRL. A BMDO project has also been jointly funded with Sanders and Cornell. Using measurements and concepts developed on this MURI, a study of the relative power performance of the AlGaN/GaN HEMT's, and SiC MESFET's was made for, and reported to Stanford Telecommunications.

II. DEVICES

A. Summary – Lester F. Eastman

AlGaN/GaN HEMT's on sapphire are yielding state-of-the-art results of > 4 W/mm for single gate devices, and > 2 W/mm for large periphery devices with 50 μm pitch between channels. Electron beam lithography has been used until now, to avoid the exposure of the AlGaN to KOH during photolithography. A new process is in development to allow photolithography throughout the processing, except for the gates. When this process is on line, much less time and expense will be required for complete HEMT processing. One aspect of the process development has been to achieve sharply reduced amount of current slump (DC to RF dispersion). AlGaN/GaN HEMT's on SiC have shown excessive gate leakage, limiting the drain-source operating voltage to ~ 40 V on recent devices. The materials growth will be optimized to eliminate this problem. In spite of this limitation, large periphery HEMT's on SiC have yielded output power levels of ~ 4 W/mm. Detailed experimental investigations of the properties of polarization-induced electrons in AlGaN/GaN HEMT structures are presented. Means of controlling the electron density

and mobility in these structures are presented for use in optimized, reproducible HEMT performance. The Static Induction Transistor (SIT) process has been developed, and initial devices have been fabricated. The materials used to date had either < $10^{16}/cm^3$ or > $10^{17}/cm^3$ doping, yielding poor current, and high gate leakage respectively. Material in the mid < $10^{16}/cm^3$ will be obtained and processed to try to achieve good SIT characteristics. A model for the non-linear properties of the HEMT's has been made, and it agrees well with experiments. Using a dual gate cascode approach, an increase of gain (10 db) with good output power and efficiency has been achieved. Circuit configurations using the non-linear model have been designed and simulated. A set of power cells will be imbedded into these circuit configurations to achieve broadband power amplification.

B. Processing - Vinayak Tilak, Kenneth Chu

We have upgraded a process for fabricating HEMT structures from AlGaN/GaN layers. The issues involved are determining good dry etches for AlGaN/GaN and working out the optimized ohmic metalization scheme. The processing can be divided into 4 levels - mesas, ohmic pads and gates.

Mesa Level

This is the first level of processing on the AlGaN surface. This is done using photolithography. The etch mask used is photoresist. This is patterned using a 5X stepper. Then the sample is etched using an electron cyclotron resonance machine. A combination of Cl_2 (12 sccm), CH_4 (3.8sccm), O_2, gases and 400 W of microwave power is used. Typically the etch lasts from 90s-120s and an etch rate of 1400 A/s is observed. The tradeoff's involved in the etch times is that if it is too shallow then there could be mesa isolation problems and if it is too deep then it could cause the gates, which have to climb the mesas, to disconnect. The etch gives straight walls and is very selective.

Ohmic Level

Initial experiments suggested that the developers used in photolithography, which are bases, etch the AlGaN preferentially where dislocations meet the surface and reduce the 2 dimensional electron gas. So, the process from this level on was done using electron beam lithography that uses solvents as developers. The ohmic patterns are written with varying source-drain spacing so that we could investigate the effects of source drain spacing on device characteristics like break down voltage. The ohmic metals used are Ti (200 A)/Al (1000 A)/Ti (450 A)/Au (550 A). The metals are annealed at 800° C(see figure 1). 800°C is chosen instead of 900°C to prevent surface damage. We can see that surface damage is minimal because the sheet resistance remains the same before and after the anneal. Typical contact resistances obtained are 0.6 Ωmm and specific contact resistance of 3.44 x 10^{-6} Ωcm^2 are obtained using this process. However, there is a problem of edge acuity as the annealing roughens the metal and causes spillage. This problem is being addressed now. Various schemes like Ti/Al/Ni/Au are being currently tried. However, we have not yet got as good an ohmic contact as with the Ti/Al/Ti/Au.

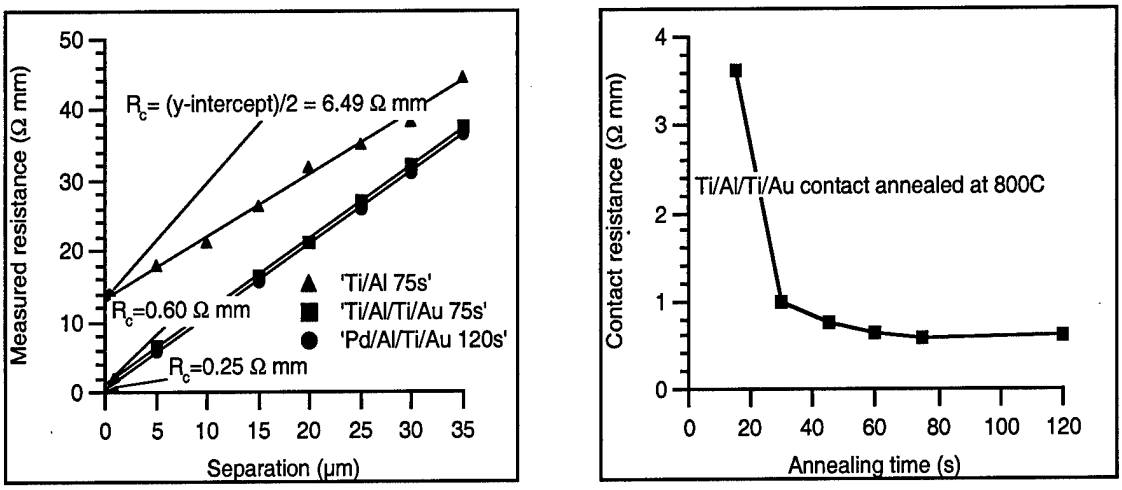

Figure 1. TLM measurement of ohmic contact resistance on AlGaN/GaN HFET layers

This past year we have started another effort in trying to develop a process using photolithography to make the ohmic contacts. The advantages being it is cheaper and less time consuming. This is done by first putting down a layer of PMMA (an e-beam resist) and flood exposing it with UV and then evaporating a 300Å layer of chromium. On this Cr the photoresist is spun and lithography is done. Then the photoresist is developed and then a Cr etch is done. Then the pattern is transferred to the surface by developing the PMMA using toluene, which selectively dissolves PMMA. This gives our undercut profile for lift off purposes shown in figure 2.

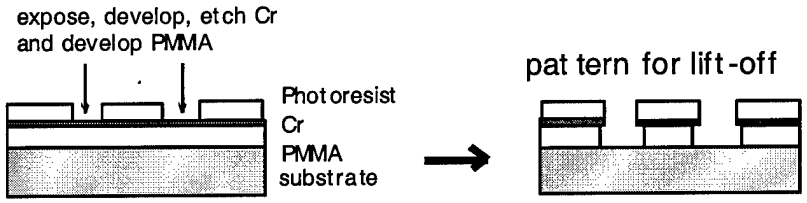

Figure 2. Multi-layer resist scheme for lift-off process using optical patterning

This process is currently being evaluated using an MBE sample.

Pads

The pads are currently being made by e-beam lithography, but this level is also being shifted to the PMMA process being discussed above. The metal used for pads is Ti(150 Å)/Au(3000 Å). There could be some problems with this metalization scheme, as it has been found recently that the contact resistance when measured from the actual devices which have pads on them seems to be about 1.5 Ωmm as compared to the TLM measurement of contact resistance which gives about 0.6 Ωmm. This could possibly be

due to the devices and TLM patterns being in different regions of the wafer, or due to a thin layer of Aluminum oxide forming on the ohmic contacts when it diffuses out during annealing. Further measurements are being carried out to reach a conclusion. This higher source-drain resistance causes the knee voltage to be higher than what it should be.

Gates

This level is done by e-beam to get the mushroom shape required for gates with gate lengths < 0.5μm. This is done with a three layer resist to facilitate liftoff and get the mushroom profile and by using area and line doses. The Schottky barrier used is Ni, and a gold layer is put on top to prevent oxidation.

Results

This process has been used successfully to make HEMT's on sapphire. We have achieved f_t's of 75 GHz and f_{max} of 140 GHz. The power output of the device also has been at the state-of-the-art with the 75μm devices on sapphire putting out 4.1W/mm of normalized power at 41% PAE. A typical I-V curve for a HEMT is shown in figure 3 along with frequency response. The initial devices on SiC, however, seem to have low break down voltages of 40 V. We are currently trying to understand why.

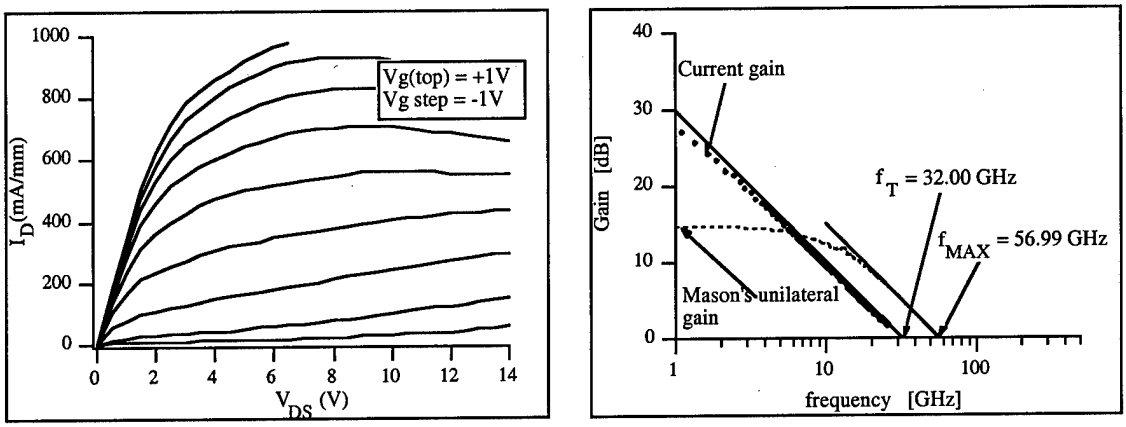

Figure 3. (a) DC characteristics of the AlGaN/GaN MODFET's showing drain current over 1 A/mm, and (b) RF performance of a 75 μm periphery device with .3 μm gate length.

The future direction of the project is to develop a quick process so those transistors needed for MMIC amplifier circuits can be fabricated reliably and cheaply. Also, we will investigate various metalization schemes for ohmic contacts to prevent roughening up of the metal surface after annealing. Any strange behavior of the contact resistance due to putting down of the pads will also be investigated and corrected. .

C. Experimental investigations of electrical transport properties of polarization induced two dimensional electron gases in Ga- and N-face AlGaN/GaN structures - O. Ambacher, R. Dimitrov, and M. Murphy

Abstract

Nominally undoped GaN/$Al_xGa_{1-x}N$/GaN high electron mobility transistor structures were grown by plasma-induced molecular beam epitaxy (PIMBE) and metalorganic chemical vapor deposition (MOCVD) in order to study the formation and electric transport properties of polarization induced two-dimensional electron gases. By depositing an AlN nucleation layer on sapphire substrates before the growth of a GaN buffer layer by PIMBE, we were able to change the polarity of the wurtzite films from N- to Ga-face. High quality Ga-face AlGaN/GaN heterostructures were grown and investigated for comparison. The switch in polarity causes a change in sign of the spontaneous and piezoelectric polarization directed along the c-axis of the strained AlGaN barrier. As a consequence the polarization induced two dimensional electron gas is confined at different interfaces in heterostructures of different polarities. The electron transport properties of two dimensional electron gases in Ga and N-face polarity heterostructures were investigated by a combination of C-V profiling, Hall effect and Shubnikov-de Haas measurements. Dominant electron scattering mechanisms are studied in order to provide the knowledge necessary for further improvements of the electric transport properties and performance of AlGaN/GaN based „normal" and „inverted" high electron mobility transistors.

1. Introduction

The ability to achieve two-dimensional electron gases (2DEGs) with sheet carrier densities of 10^{13} cm^{-2} or higher at the interface of nominally undoped AlGaN/GaN heterostructures is caused by polarization induced bound interface charges [1-3]. Wurtzite GaN, AlN and their alloys are highly piezoelectric and show strain independent spontaneous polarization along the c-axis [4]. The direction of the piezoelectric and spontaneous polarization is determined by the polarity of the material (N-face or Ga-face), which for PIMBE growth can be controlled by the deposition of an additional AlN nucleation layer [5]. High structural quality AlGaN/GaN heterostructures grown on AlGaN nucleation layer by MOCVD are found always to be Ga-face [6]. The total polarization in the AlGaN barrier of the transistor structure is the sum of the piezoelectric and spontaneous polarization. Both kinds of polarization increase with the fraction of aluminum in the pseudomorphically grown AlGaN layer on top of a thick GaN buffer and point toward the sapphire substrate (or surface) for Ga-face (or N-face) polarity crystals [7]. The abrupt change of polarization on passing from the AlGaN to the GaN causes a bound sheet charge density located at either AlGaN/GaN interface. If this charge is positive, free electrons are attracted to compensate this charge by forming a 2DEG in the GaN close to the interface.

Our recent investigations were focused on the structural and electrical transport properties of AlGaN/GaN based heterostructures grown by plasma-induced molecular

beam epitaxy (PIMBE) or metalorganic chemical vapor deposition (MOCVD). Heterostructures with Ga-face and N-face polarity, and with different Al mole fraction of the barrier were compared to investigate the important role of polarization induced effects for the carrier confinement. Enabled by a significant improvement of structural quality of Ga-face *and* N-face heterostructures a study of electrical transport properties of polarization induced 2DEGs was carried out by a combination of CV-profiling, Hall effect and Shubnikov-de Haas measurements.

2. Experimental

To investigate the structural quality of AlGaN/GaN heterostructures, we have used atomic force microscopy (AFM), high resolution X-ray diffraction (HRXRD) measurements. The structural quality and surface morphology of the GaN buffer layer improved with increasing thickness. We observed a rms surface roughness of 5 nm by AFM (Fig. 2) and a FWHM of the (00.2) XRD rocking curve of 250 arcsec for N-face polarity GaN buffer layers with a thickness of 2 μm grown directly on sapphire without intentional nitridation or depositing a nucleation layer. For these undoped GaN buffer layers, background doping levels of $5x10^{16}$ cm^{-3} and electron mobilities of 520 cm^2/Vs were measured at room temperature. A free carrier concentration of $5x10^{16}$ cm^{-3} in the GaN buffer layer yields a sheet carrier concentration of $1x10^{13}$ cm^{-2}, which can lead to a significant reduction of the cut off frequency of AlGaN/GaN based polarization induced high electron mobility transistors (PI-HEMTs) by inductive coupling to the 2DEG. Therefore we deposited a semi-insulating GaN buffer layer by compensating the free electron concentration with magnesium. By fine tuning of the Mg-flux the free carrier concentration was reduced to values below $1x10^{14}$ cm^{-3}.

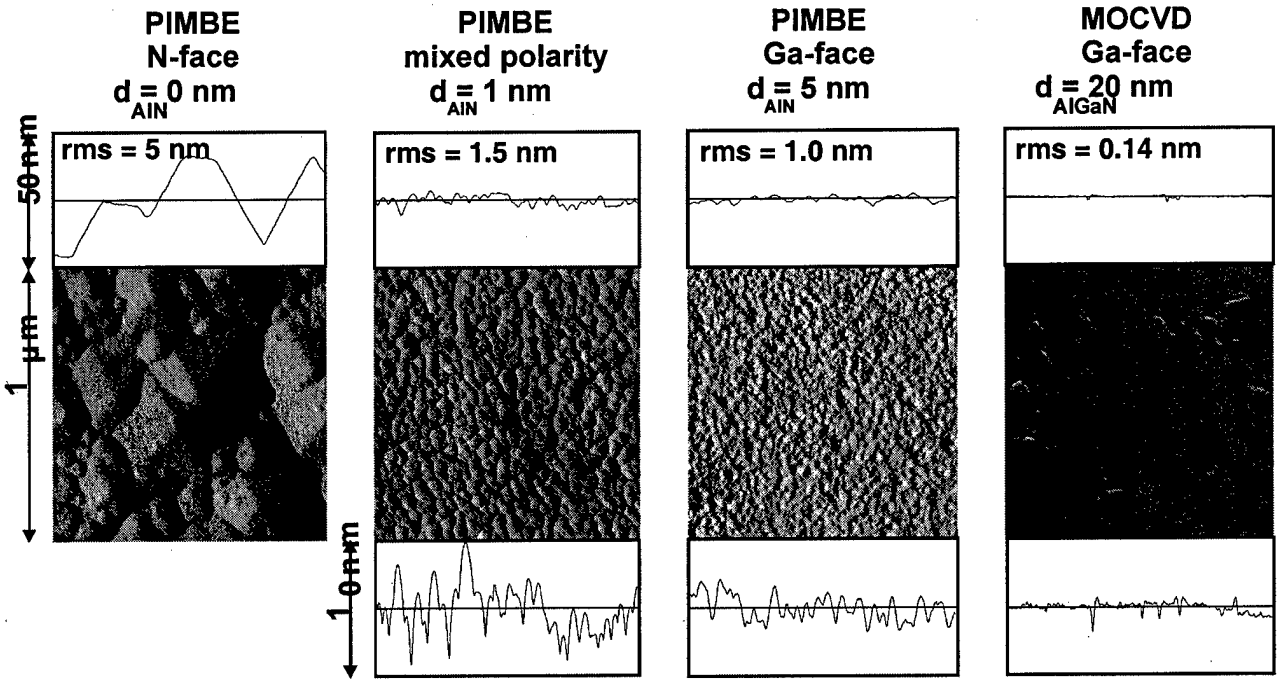

Figure 1: *AFM measurements of N-face and Ga-face GaN buffer layer grown by PIMBE on AlN nucleation layer different thicknesses. An AFM picture of Ga-face GaN deposited by MOCVD is given for comparison.*

GaN buffer layers with Ga-face polarity were grown by PIMBE using an AlN nucleation layer. The nucleation layer was grown at 800°C for about *40*-90 s with a typical deposition rate of 0.4 μm/h. The use of this nucleation layer resulted in insulating GaN buffer layers ($n_e < 10^{15}$ cm^{-3}) without any additional compensation by Mg acceptors. For GaN layers grown without and with an AlN nucleation layer, we observed the deposition rate to be 0.45 and 0.42 μm/h, respectively. With HRXRD of the symmetrical (00.2) reflections, we were not able to determine a significant difference in the structural quality of GaN grown with and without a nucleation layer. On the other hand, AFM measurements showed quite different surface morphologies of the GaN buffer layers (Fig.1). For GaN grown without AlN nucleation layer AFM images indicated three-dimensional island growth and a diameter of the wurtzite crystals of about 500-1000 nm. We achieved a rms surface roughness of 5 nm over an area of 100 μm^2. The use of the AlN nucleation layer gave rise to a decrease of the diameter of the crystals to about 50 nm and of the rms roughness to about 1 nm over the same surface area (Fig. 1). The MOCVD grown undoped Ga-face AlGaN/GaN heterostructures were deposited at a pressure of 100 mbar, using triethylgallium (TEG), trimethylaluminium (TMA) and ammonia as precursors. A growth rate of about 0.5 μm/h was achieved for a substrate temperature of 1040°C [6]. The AlGaN/GaN heterostructure as well as the $Al_{0.1}Ga_{0.9}N$ nucleation layer were grown at a constant substrate temperature and without any growth interruptions to avoid the presence of excessively high free carrier background concentrations. AFM measurements showed a crack free surface morphology with bilayer steps causing a root mean square surface roughness below 0.2 nm for HEMT structures grown using AlGaN nucleation layers with a thickness of about 20 nm.

To study the formation and electrical transport properties of 2DEGs in heterostructures with different polarities we have deposited two kind of structures, differing in the initial stage of growth. The first type of structure consists of a 2 μm thick N-face GaN buffer layer grown directly on sapphire substrate, an undoped $Al_xGa_{1-x}N$ Barrier with thickness of 20 nm, and an undoped GaN channel on top (inverted HEMT). The second type of transistor structure was deposited by applying the same growth conditions mentioned above, but including a thin AlN nucleation layer as the first growth step to achieve Ga-face polarity material. To fabricate normal HEMT structures, undoped $Al_xGa_{1-x}N$ ($0.1<x<0.45$) barriers with thicknesses between 20 and 30 nm, and a 2.5 nm thin GaN cap layer were deposited on top of the buffer layer.

3. Results and Discussion

In order to determine the polarity of the HEMT structures, we evaluated the carrier concentration profiles and the location of the 2DEGs inside heterostructures of both types

by C-V profiling measurements. For structures grown without an AlN nucleation layer, the 2DEG was confined at the upper interface of the AlGaN barrier, in contrast to structure grown with an AlN nucleation layer, where the 2DEG was located at the lower AlGaN/GaN interface (Fig. 2). This result is in agreement with references 2 and 5 showing that the polarity of the heterostructures is flipped from N-face (inverted heterostructure) to Ga-face (normal heterostructure) by inserting a thin AlN nucleation layer.

An increase of sheet carrier concentration with increasing Al-concentration of the barrier was determined by a combination of Hall, C-V profiling and HRXRD as reported earlier [1, 3]. By example, an increase of sheet carrier density from $0.45x10^{13}$ to $1.1x10^{13}$ cm^{-2} by increasing the Al concentration from x =.0.23 to 0.37 was observed for N-face heterostructures. By increasing the Al concentration of the barrier layers, the strain induced piezoelectric polarization as well as the spontaneous polarization (having the same direction as the piezoelectric polarization for tensile strained barriers) are increased. As a result, the amount of polarization induced sheet charge and therefore the induced sheet carrier concentration located at one of the AlGaN/GaN interfaces is increased.

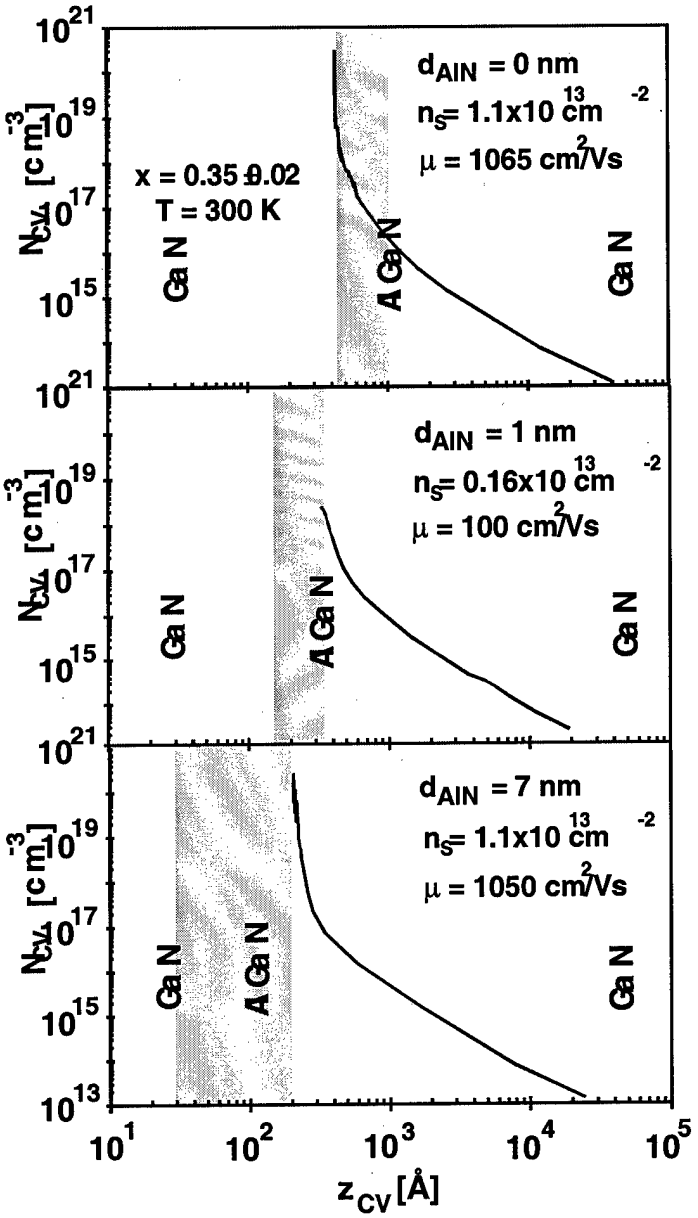

Figure 2: *C-V profiling measurements of GaN/AlGaN/GaN heterostructures grown by PIMBE without an with AlN nucleation layers of 1 and 7 nm thickness. The 2DEG in the heterostructure without nucleation layer is confined at the upper GaN/AlGaN interface indicating N-face polarity (inverted HEMT). Ga-face heterostructures with 2DEGs confined at the lower AlGaN/GaN interface are observed for samples with AlN nucleation layers with a thickness above 7 nm.*

By room temperature Hall effect measurements we observe the highest 2DEG mobilities for N-as well as for Ga-face HEMT structures at sheet carrier concentrations close to $5x10^{12}$ cm^{-2}. For N- and Ga-face heterostructures grown by PIMBE the highest mobilities are 1215 and 1236 cm^2/Vs (T = 300 K), respectively. For Ga-face MOCVD grown

structures mobilities up to 1575 cm^2/Vs were achieved. For higher sheet carrier concentrations and both polarities grown by PIMBE or MOCVD, we measured a decrease of the 2DEG mobility (Fig. 3).

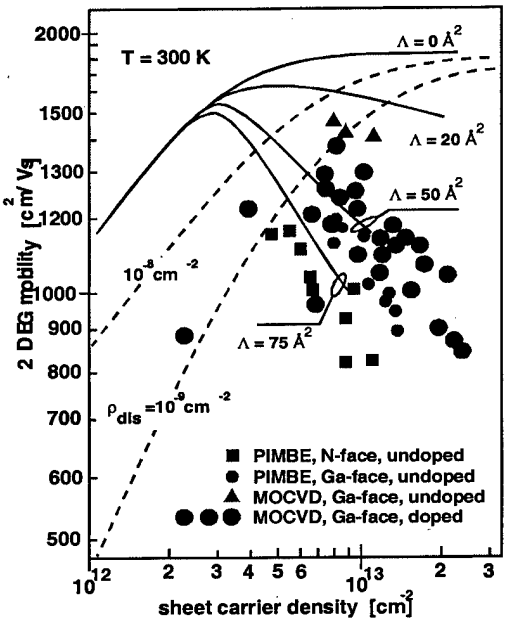

Figure 3: *Room temperature 2DEG Hall mobilities of N- and Ga-face AlGaN/GaN heterostructures grown by PIMBE or MOCVD versus sheet carrier concentration. The solid lines are predicted 2DEG mobilities for HEMT structures with different interface roughnesses. The dashed lines indicate the additional reduction of mobility by scattering due to charged dislocations with densities of 10^8 and 10^9 cm^{-2}.*

This observation is also in agreement with the experimental results by Gaska et al. [8] and can be explained by interface roughness scattering. The sheet carrier concentration of polarization induced 2DEGs is increased by increasing the Al-concentration of the barrier. At the same time the polarization induced bound interface charge is increasing and the average distance between the 2DEG and the AlGaN/GaN interface becomes smaller and smaller (below 20 Å for $x > 0.25$). As a consequence interface roughness scattering becomes a limiting factor for the 2DEG mobility. In Fig.3 (solid lines) the theoretical predictions for the room temperature 2DEG mobilities are shown for AlGaN/GaN interfaces with different roughnesses. For HEMT structures with low sheet carrier concentrations ($n_s < 0.5 \times 10^{13}$ cm^{-2}) electron scattering due to charged threading dislocations is predicted to be important. For HEMTs with low sheet carrier

concentrations of $0.3x10^{13}$ cm^{-2} and typical dislocation densities, ρ_{dis}, of 10^8 and 10^9 cm^{-2}, a reduction of mobility by 20 and 40%, respectively, is calculated.

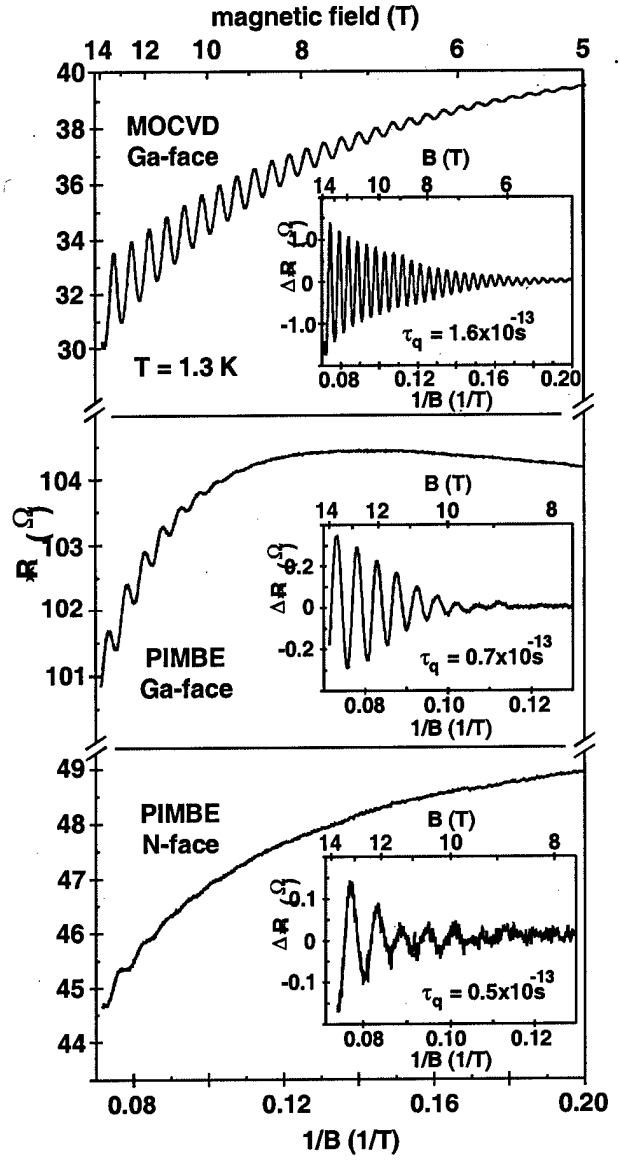

Figure 4: *Shubnikov-de Haas measurements of Ga- and N-face AlGaN/GaN HEMT structures grown by MOCVD or PIMBE.*

The presence of two-dimensional electron gases in Ga- and N-face heterostructures were confirmed by high magnetic field transport measurements up to 14 T at 1.3 K. Shubnikov-de Haas oscillations of the magnetoresistance R_{xx} were well observed above 9 T for the Ga-face PIMBE and MOCVD heterostructure (Fig.4). In spite of the lower Hall mobility at 1.3 K the SdH oscillations in the N-face material were very weak and only detectable at high magnetic fields. The magnitude of the SdH oscillations relies on the

quantum scattering time τ_q. The higher amplitude of the SdH oscillations in the case of the Ga-face samples indicates longer quantum scattering time and better electrical transport properties in comparison to the N-face HEMTs. The 2DEG mobilities, quantum and transport scattering times, τ_t, obtained by Hall effect and SdH measurements are summarized in Tab.1.

Table 1: *Sheet carrier concentration, 2DEG mobility, quantum and transport scattering time of N- and Ga-face heterostructures grown by PIMBE and MOCVD.*

	PIMBE		MOCVD	PIMBE
	Ga-face		Ga-face	N-face
n_s(300 K)	[10^{13} cm^{-2}]	0.87		0.81
	1.05			
μ(300 K)	[cm^2/Vs]	1215		1236
	1575			
μ(1.3 K)	[cm^2/Vs]	3450		4100
	4500			
τ_p(1.3 K)	[10^{-13} s]	0.5		0.7
	1.6			
τ_t(1.3 K)	[10^{-13} s]	4.5		5.3
	5.8			
τ_t/τ_p				8.9
7.6			3.6	

4. Conclusion

The following conclusions can be extracted from the measured structural and electrical transport properties of N-face and Ga-face HEMTs grown by PIMBE and MOCVD:

- N-face GaN grown by PIMBE has to be compensated by Mg to achieve high insulating buffer layers.
- The structural and interface quality of state of the art Ga-face heterostructures grown by MOCVD is higher than of Ga-face AlGaN/GaN HEMTs deposited by PIMBE.

- The highest 2DEG mobilities in Ga-face and N-face AlGaN/GaN heterostructures are achieved for sheet carrier concentrations of $5x10^{12}$ cm^{-2}. Interface roughness scattering and scattering due to charged dislocations are the limiting factors of the 2DEG mobility for high and low sheet carrier concentrations, respectively.
- SdH measurements indicate small angle scattering to be dominant ($\tau_t > \tau_p$) at low temperatures for samples with sheet carrier concentrations of about $1x10^{13}$ cm^{-2}.

Further improvement of the electrical transport properties and performance of AlGaN/GaN HEMTs requires further reduction of the dislocation density ($n_s < 1x10^8$ cm^{-2}) and smoother interfaces ($\Lambda < 10$ $Å^2$).

References

[1] O. Ambacher, J. Smart, J. R. Shealy, N. G. Weimann, K. Chu, M. Murphy, W. J. Schaff, L. F. Eastman, R. Dimitrov, L. Wittmer, M. Stutzmann, W. Rieger and J. Hilsenbeck, J. Appl. Phys. **85** (1999) 3222.

[2]R. Dimitrov, A. Mitchell, L. Wittmer, O. Ambacher, M. Stutzmann, J. Hilsenbeck and W. Rieger, Jpn. J. Appl. Phys. **38** (1999) 4962.

[3] O. Ambacher, B. Foutz, J. Smart, J.R. Shealy, N.G. Weimann, K. Chu, M. Murphy, A.J. Sierakowski, W.J. Schaff, L.F. Eastman, R. Dimitrov, A. Mitchell, and M. Stutzmann, .J. Appl. Phys. in print (1999).

[4] F. Bernardini and V. Fiorentini, Phys. Rev. B **56** (1997) R10024.

[5] M. J. Murphy, B. E. Foutz, K. Chu, H. Wu, W. Yeo, W. J. Schaff, O. Ambacher, L. F. Eastman, T. J. Eustis, R. Dimitrov, M. Stutzmann, and W. Rieger, Mat. Res. Soc. Symp. Proc. Fall Meeting, Boston, Dec. 1998, in print.

[6] J.A. Smart, A.T. Schremer, N.G. Weimann, O. Ambacher, L.F. Eastman, and J.R. Shealy, Appl. Phys. Lett. **75** (1999) 388.

[7] R. Dimitrov, L. Wittmer, H. P. Felsl, A. Mitchell, O. Ambacher, and M. Stutzmann, phys. stat. sol. (a) **168**, R7 (1998).

[8] R. Gaska, M.S. Shur, A.D. Bykhovski, A.O. Orlov, G.L. Snider, Appl. Phys. Lett. **74**, 289 (1999).

D. GaN Static Induction Transistor fabrication - Nils Weimann

With the super-self aligned GaN SIT fabrication process developed at Cornell University, we were able to demonstrate for the first time a GaN Static Induction Transistor. The resulting drain characteristics for a multifinger SIT are shown in Figure 1.

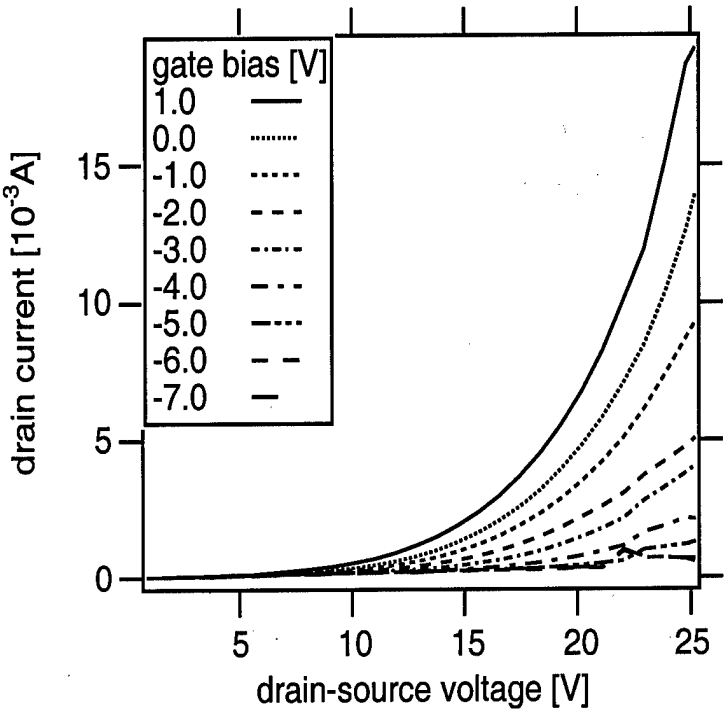

Figure 1: drain characteristics of a 25 x 75 µm SIT, wafer IAF-510

The device has a total periphery of 1.875 mm, consisting of 25 fingers of 75 µm length each. The maximum drain current at 25 V_{DS} scaled to the periphery of the device[1] is 10.7 mA/mm, corresponding to a current density of 668 A/cm^2. The source finger width is 1.6 µm, the vertical gate length 0.3 µm, and the gate-source spacing 0.5 µm. The drift region thickness is 2.2 µm. The drift region is unintentionally doped with a carrier concentration less than 10^{16} cm^{-3}. The large onset voltage of 10 V is due to the low carrier concentration in the drift region, which leads to mainly space-charge limited current flow.

A blocking voltage gain of 25/7 = 3.57 was achieved. The DC curve family in Figure 1 was measured on a pulsed setup, the total pulse duration was 100 msec with a duty cycle of 1%. The devices are laid out in a common-drain configuration, which did not allow us to measure small-signal gain. The yield of working devices per chip is around 50%, which is high given the complexity of the vertical transistor process, and the large device peripheries.

To increase the drain current, a set of doped SIT structures was grown by MOCVD at Fraunhofer-IAF. The devices processed on these wafers did not show an onset voltage. However, the Ni Schottky diodes on the etched surfaces of the moderately doped material ($\approx 10^{17}$ cm^{-3}) were very leaky. It was not possible to pinch off these devices. The high leakage current may be due to the gate metal filled etch pits on the bottom of the gate

[1] One unit length device periphery includes one unit length of both left and right hand side edges of the source finger

trench, which effectively shunt the Schottky barrier. The barrier width is much smaller in the case of the doped drift region.

In summary, over the three years of the GaN SIT project, we developed a process which allows to fabricate GaN SIT devices at sufficient yield. Annealed Hf/Au ohmic contacts on n^+ GaN with a specific contact resistance of $< 10^{-5}$ Ωcm^2 were fabricated routinely. Ni Schottky contacts on unintentionally doped GaN with a leakage current of less than 1 A/cm^2 at -10 V_{GS} were fabricated. A combined ECR dry- and KOH wet etch process which yields smooth vertical features was developed. Further improvements require better control of the doping concentration in the drift region, and the suppression of the gate leakage.

E. Circuits - Bruce Green

Development of a process for high-power, broadband amplifiers based on AlGaN/GaN HEMT technology include results on 1) an accurate analytical large signal model for the AlGaN/GaN devices, 2) process development for power optimization of the HEMTs, and 3) initial results on dual gate amplifier cells implemented in this process.

Nonlinear Device Model

The model used for circuit design consists of a Curtice-cubic analytical model with the introduction an additional current source to account for positive g_m dispersion arising from trapping effects in the devices. A 4 GHz loadpull validation of this model showing good agreement between the measured and modeled power characteristics for 50 Ω source and load terminations is shown in Figure 1.

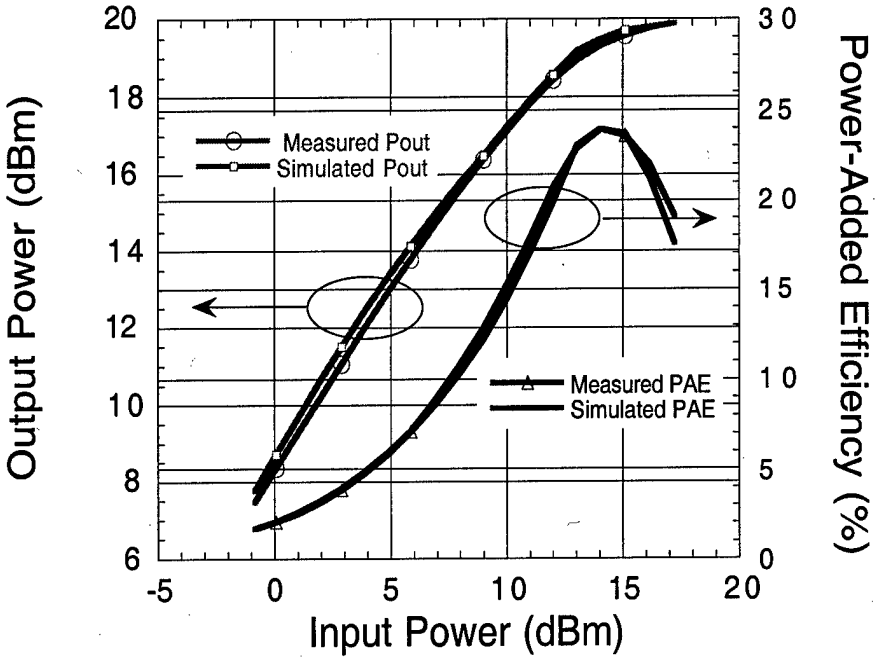

Figure 1: Loadpull validation of nonlinear HEMT model used for circuit design (V_D=4 V, V_G=-4 V, Z_S=Z_L=50 Ω). Gate length is .45 µm, and periphery is 250 µm.

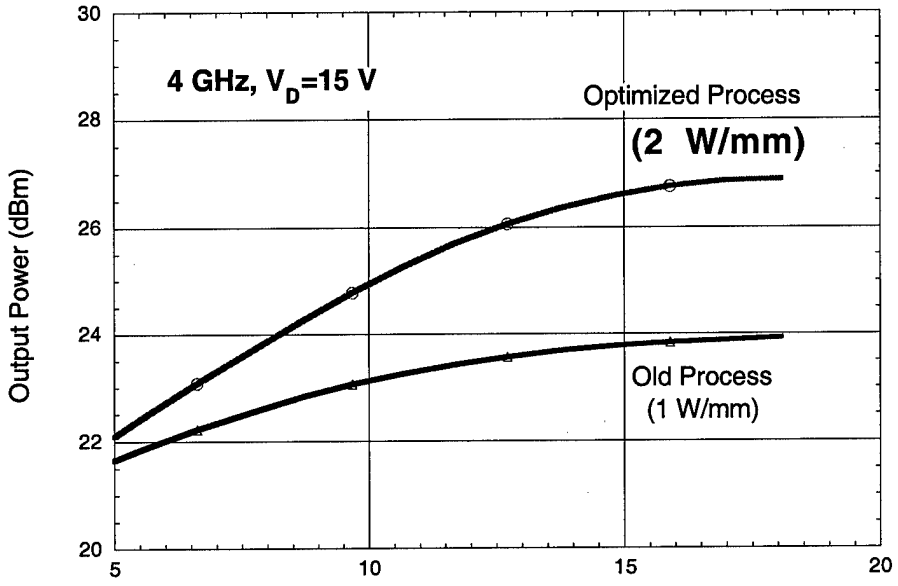

Figure 2: Illustration of the influence of processing on large signal performance of 2X125X0.5 μm devices fabricated on identical AlGaN/GaN/sapphire epilayer structures with changes only in the device processing steps.

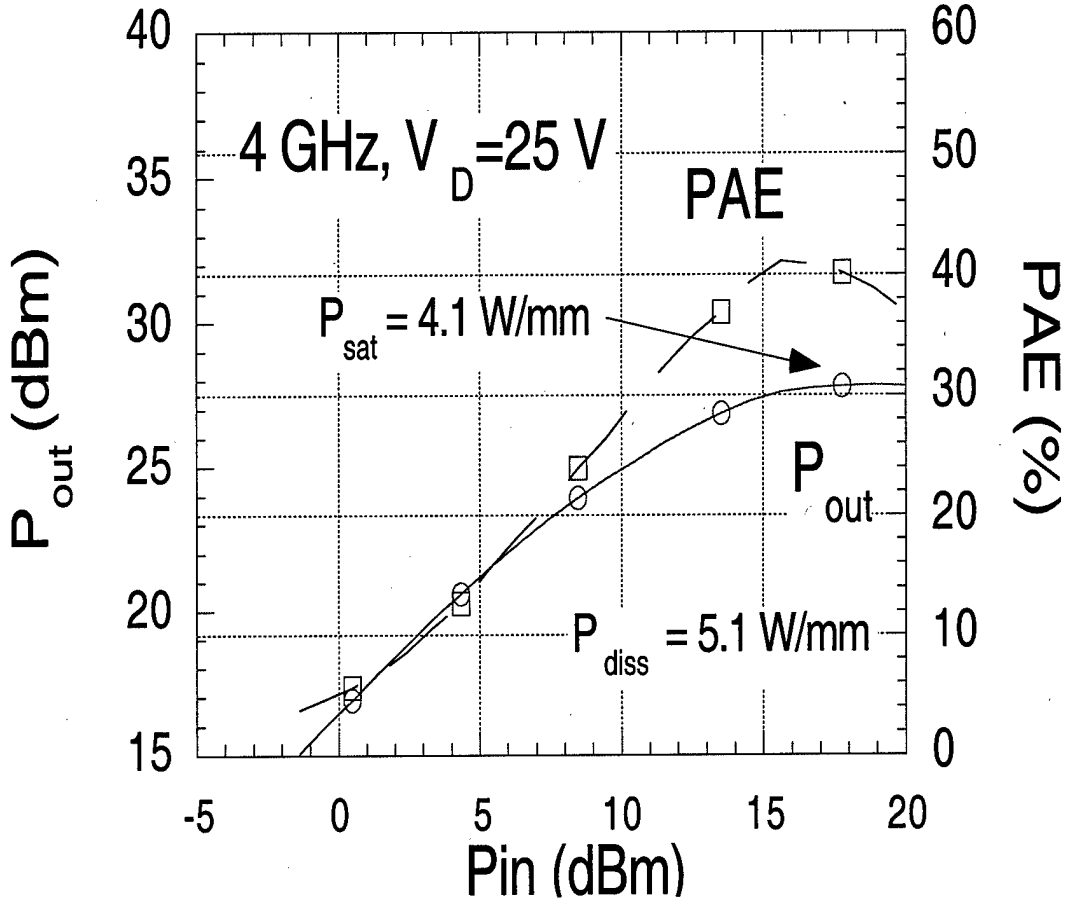

Figure 3: Large signal characteristics of 2X75X0.5 μm AlGaN/GaN HEMT on sapphire substrate.

Process Optimization

Research in processing methods for AlGaN/GaN devices has led to discoveries of processing methods that minimize or eliminate the presence of currently slump (DC-RF dispersion) in the devices. Figure 2 illustrates an improvement in saturated power density from 1 W/mm to 2 W/mm (V_D=15 V) obtained through these improvements in processing. This figure illustrates that by changing only the device process for HEMTs fabricated from material of the same growth run, a twofold increases in power performance have been obtained. Figure 3 shows the saturation characteristics of a 2X75x0.5 μm HEMT on sapphire measured at 4 GHz with a drain bias of 25V yielding a

4.1 W/mm power density. Further details of the processing techniques and physical models relevant to these results will be the subject of future reports.

Example: Dual Gate Amplifier Cells

Using this improved MMIC process, dual gate amplifier cells were fabricated using AlGaN/GaN HEMTs on SiC substrates. These devices were fabricated for opimization of breakdown voltage and frequency response by employing a 0.25 μm gate length for the common source device for high current gain and f_T and a 0.4 μm common gate device for an increased breakdown voltage. The small-signal measurements of Figure 4 show an 8 dB increase in maximum stable gain over a common source device of the same dimensions (.25 μm gate length) elsewhere on the wafer. A power density of 4 W/mm (total power 1 W) at 4 GHz was achieved at a drain bias of 25 V as shown in Figure 5. This result sets the state of the art power for AlGaN/GaN based dual gate HEMTs.

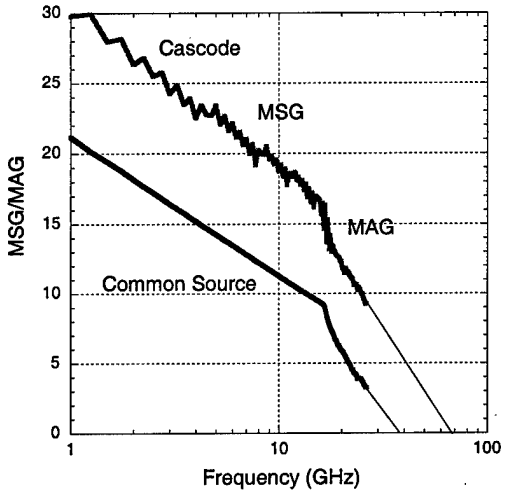

Figure 4: Comparison of maximum stable gain (MSG)/ maxi mum available gain (MAG) for a L_{g1}=.25 μm, L_{g2} = .4 μm dual gate FET and a L_g=0.25 μm common source device. Both devices have a gate periphery of 250 μm.

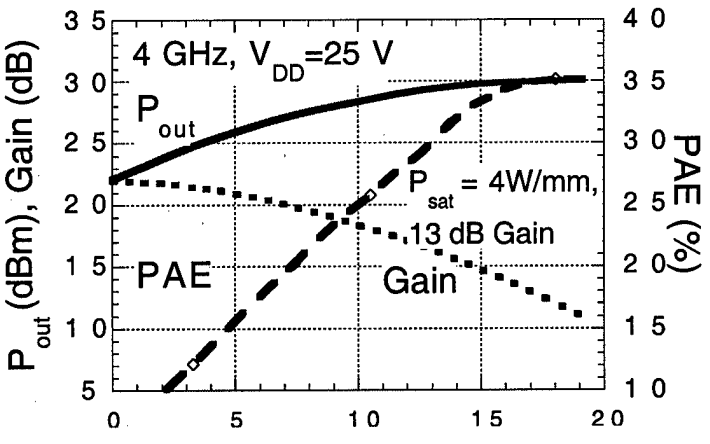

Figure 5: Large signal characteristics of fabricated 2X125 μm dual gate HEMT amplifier cell.

F. GaN Amplifier Design - K. J. Webb, Purdue University

The effort at Purdue has focussed on a design and experimental program that will culminate in a GaN broadband monolithic microwave push-pull Class B distributed power amplifier. Several key concepts have been addressed during 1998/99 to pave the way to achieve this goal, and the success in these areas is outlined.

The first monolithic distributed amplifier was designed, built and tested in collaboration with Cornell. This amplifier operated in Class A and was designed using an optimization strategy that resulted in elimination of the drain-line dummy load and a concomitant increase in efficiency. It used CPW realizations of inductors for both the gate and drain lines. Subsequent simulations of improved non-uniformly distributed amplifier designs, an example of which is shown in Fig. 1, show a 10% increase in efficiency across the entire band over that achievable with a standard uniformly distributed amplifier. This is an important step in order to be able to achieve the high efficiency requirement for the push-pull amplifier, and removal of the dummy drain load that was suggested in the MURI program goals.

In order to achieve both high output power and broad bandwidth (i.e., high frequency) operation from a distributed amplifier, it is necessary to have distributed gain cells, each of which have cascaded HEMTs. A comparison between Darlington, cascode etc. designs using experimentally-derived FET models has yielded prime candidate approaches. A cascaded gain cell amplifier will be fabricated and tested in collaboration with Cornell.

A Class B push-pull non-uniformly distributed amplifier has been designed and stimulated to achieve PAE of 50% over 2-10 GHz with an output power of 42-47 dBm. This amplifier uses ideal transformer baluns at the input and output and has three stages in both push and pull sections. Each gain cell has two parallel 2mm periphery GaN FETs, resulting in a total periphery of 4 mm, with a broadband passive lumped-element splitter. The output is highly linear (3rd harmonic more than 20 dB down for input powers up to 40 dBm at 10 GHz). Further design is necessary in order to achieve an amplifier suitable for fabrication.

A critical element in achieving a push-pull Class B amplifier is the input and output balun. We have proposed coupling the balanced amplifier output directly into a broadband (Vivaldi) antenna. As for transmission line baluns, we have been investigating single and multi-layer designs based on the Marchand concept. Bandwidths in the neighborhood of 2-12 GHz are achievable, although being resonant structures the dimensions are large by monolithic circuit scales. We are investigating ways to make these designs suitably compact. Example baluns will be fabricated at Purdue shortly and then tested.

At the suggestion of ONR, we are pursuing a tuned push-pull Class B GaN amplifier design for operation at 10 GHz. Our hope is to fabricate and test this in the near future.

Using measured data from Cornell GaN HEMTs taken at Purdue, a distributed FET model has been used to accurately fit the data for various gate widths. This has allowed investigation of the influence of both phase shift and attenuation along the gate line for these devices.

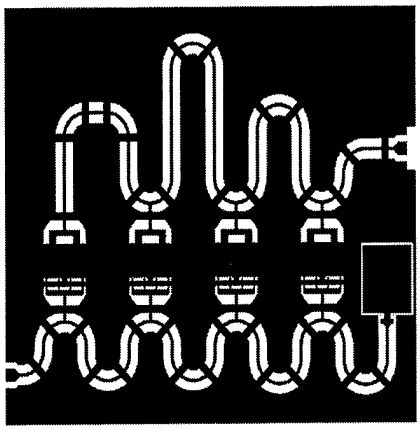

(a)

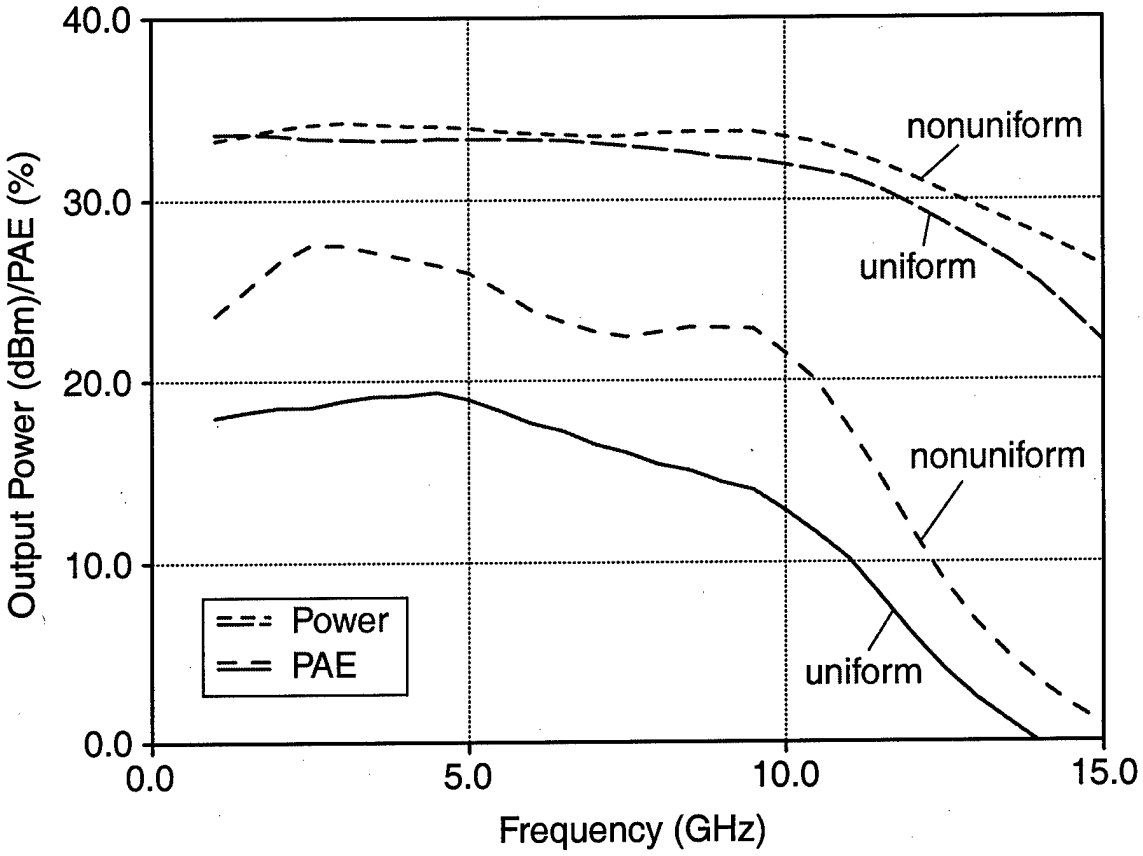

(b)

Figure 1. (a) Layout for a four stage GaN non uniform Class A monolithic distributed amplifier with no drain line dummy load for increased efficiency. Each HEMT has a 0.5 mm periphery and a 0.25 micron gate length. (b) Output power and power added efficiency for the non uniform amplifier in (a) and its uniform equivalent. Note that the uniform amplifier was optimized for maximum output power, providing a best case result for that design. The optimized non uniform result provides an increase in efficiency of approximately 10% over the best uniform design. The input power was 26.6 dBm, and V_{gs} = -2.6V and V_{ds} = 15 V.

III. THEORETICAL STUDIES AND 1/*f* NOISE

A. Summary – Lester F. Eastman

Various experimental frequency responses of AlGaN/GaN HEMT's have been compared with the electron transport properties of bulk GaN predicted by Monte Carlo analysis. The interpretation of the experimental results is more than a third lower than that predicted, even when the equal areas rule is invoked to obtain the average electron transit velocity through the high field region. If the high field region has a significant extension beyond the drain end of the gate, this would explain the discrepancy. The Monte Carlo

analysis has been developed in cooperation with Prof. M. Shur of RPI. The computer program "CBAND" has been modified to include the electrical polarization effects in predicting the 2DEG sheet density, and experimental results roughly agree. A fundamental theory of the electron mobility in the 2DEG has been completed with the electron sheet density as a parameter. It shows a limit of ~ 2,000 cm^2/V-s for ~ $4x10^{12}/cm^2$, and ~ 1,800 cm^2/V-s for ~ $1x10^{13}/cm^2$ electron sheet density. These values are somewhat conservative, since some experimental results are at least this high even in the presence of charged dislocations. $1/f$ noise has been measured in cooperation with Prof. M. Shur of RPI. He has also done modeling of the electrical polarization effects, and has developed a novel GaN-based MOSFET idea.

B. Device Modeling and Electron Transport in the group III-Nitrides – Brian E. Foutz

Monte Carlo Electron Transport

In previous years, the velocity-field characteristics and the effects of temperature and doping on that characteristic have been studied. This year, in cooperation with Prof. Michael Shur and Prof. Stephen O'Leary, the effects on transient electron transport have been examined. Our results [1] show that GaN and InN demonstrate significant velocity overshoot effects with peak electron velocities of $1x10^8$ cm/s over short distances when the applied electric field is greater than 500 kV/cm in GaN and 250 kV/cm in InN. In general, InN shows superior transport properties, exhibiting both a higher velocity-field characteristic and larger overshoot velocities over larger distances than GaN. Using a very simple model, $f_T = 1/(2\pi\tau)$, where τ is the transit time under the gate, we give an upper bound on the performance of HFETs. Figure 1 summarizes these results.

From Figure 1 we see that the performance of most HEMTs falls well below that predicted from Monte Carlo results. Taking the conservation of charge along the channel into account yields another simple model for the effective velocity of the electrons under the gate known as the Equal Areas Rule. This rule states that the effective electron velocity is the average of the velocity-field characteristics up to the peak field in the channel of the device. Figures 2 shows the Equal Areas velocity for GaN at 300 K and 550 K for peak fields of 1, 2, and 3 MV/cm, the highest field being the approximate breakdown field of GaN. In general, GaN maintains a large effective velocity even at high temperatures.

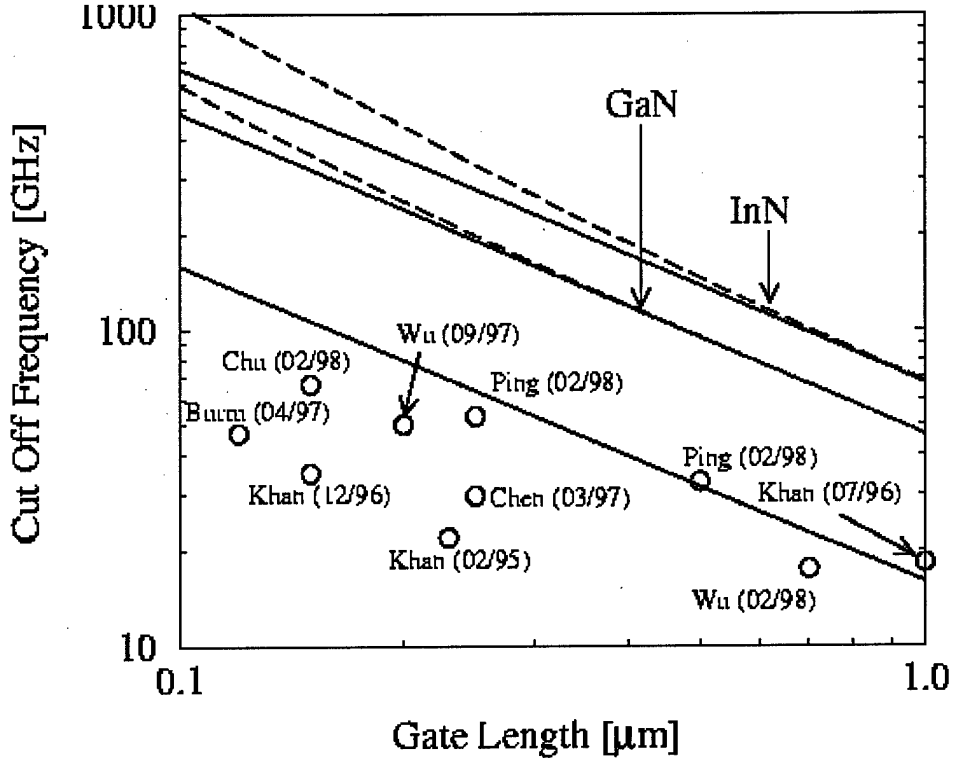

Figure 1: The dashed lines show the estimated upper bound on the cut-off frequency performance of HFETs including velocity overshoot. The solid lines show the same upper bound not including overshoot effects. The experimentally measured cut-off frequency performance for recently fabricated AlGaN/GaN HFETs are shown with the circles. Finally, the lowest solid line shows the expected performance assuming a constant electron velocity of 1.0×10^7 cm/s.

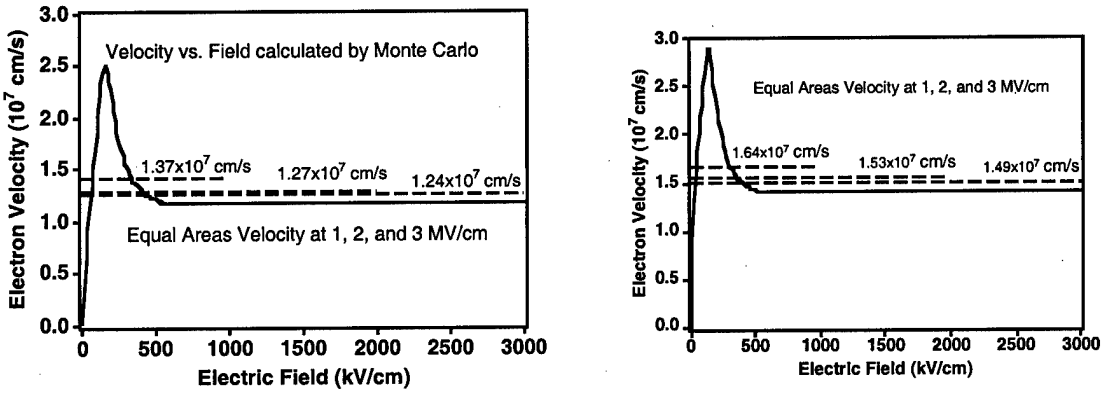

Figure 2: The Equal Areas velocity for 1, 2, and 3 MV/cm in GaN at 300 K (right) and 550 K(left).

Polarization Effects and CBAND Calculations The self-consistent Schrodinger-Poisson solver, CBAND, has been modified to
to incorporate the effects of polarization. Using the modified code to simulate the AlGaN/GaN PI-HEMT we find:

1. The 2DEG at the AlGaN/GaN interface is primarily induced by the bound charge at the interface, and less so by the conduction band discontinuity or even doping of the barrier. The component induced by spontaneous polarization is just as important, if not more important, than the piezoelectric component. The only way to achieve the electron gas concentrations measured experimentally is to include both types of polarization. See figure 3.

2. The pinch-off voltage (the gate voltage which causes the 2DEG concentration to go to zero) decreases from -2 V for a 100 Å barrier, to -8 V for a 300 Å 30% Al barrier. This effect will decrease the transconductance (and the gate capacitance) of thicker barrier PI-HEMTs.

A. Only the lowest 2DEG subband is occupied for barriers with Al concentrations up to 35% at low fields.

B. Doping the AlGaN barriers has also been studied. We find that for 30% Al barriers, polarization effects still dominate the 2DEG sheet charges even up to $1x10^{19}$ cm^{-3} doping. With no doping the sheet charge is $1.4x10^{13}$ cm^{-2} and with $1x10^{19}$ cm^{-3} doping the sheet charge only increases to $1.7x10^{13}$ cm^{-2}.

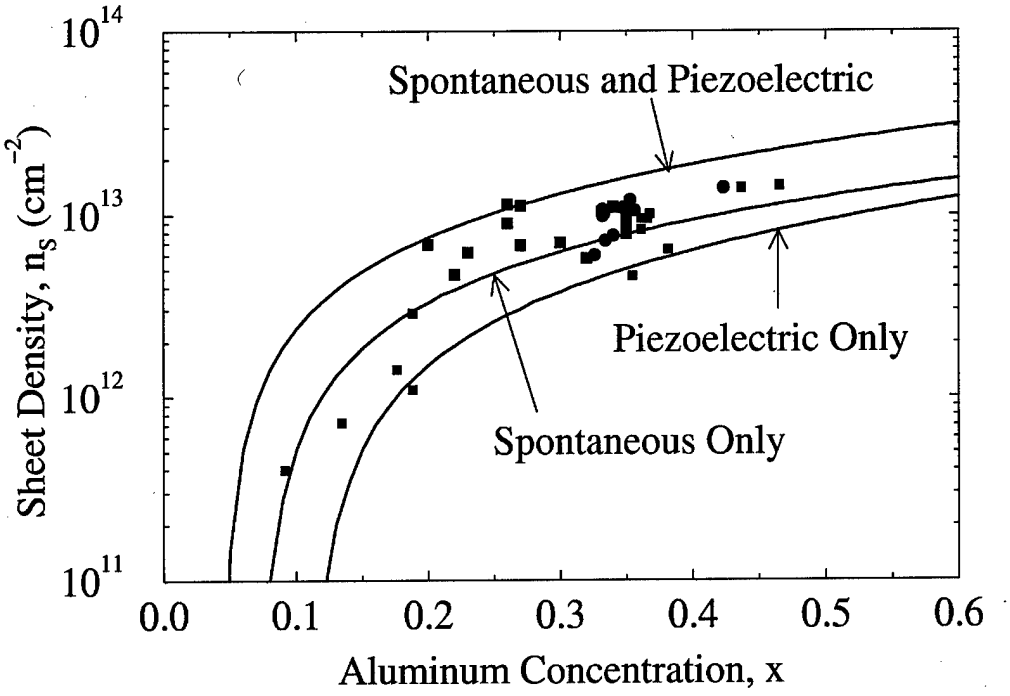

Figure 3: The sheet density vs. aluminum concentration in measured AlGaN/GaN PI-HEMT structures and the calculated sheet density calculated by CBAND. The only way to account for the measured sheet densities is to assume both spontaneous and piezoelectric polarizations contribute. The difference between the observed data and the calculation is expected to be due to differences in material quality, for example, dislocation density.

These results have been presented at the MRS Spring meeting [2] and at the Third International Conference on Nitride Semiconductors [3]. A review of the entire Y symposium (the Nitride session) at the Spring MRS Meeting was written for the June Issue of Compound Semiconductor Magazine [4].

Low Field Mobilty of the AlGaN/GaN 2DEG

Together with Prof. Brian Ridley the low-field mobility at the AlGaN/GaN interface has been calculated analytically. Included in the calculation are the polar optical phonon, piezoelectric, acoustic deformation potential, and interface roughness scattering mechanisms. The results show that, as expected, polar optical phonon scattering dominates. Surprisingly, however, piezoelectric scattering is also important, unlike many other III-V semiconductors. Figure 4 shows the low-field mobility for each component of the 2DEG mobility as a function of sheet density. These results have been submitted to Physical Review B [5].

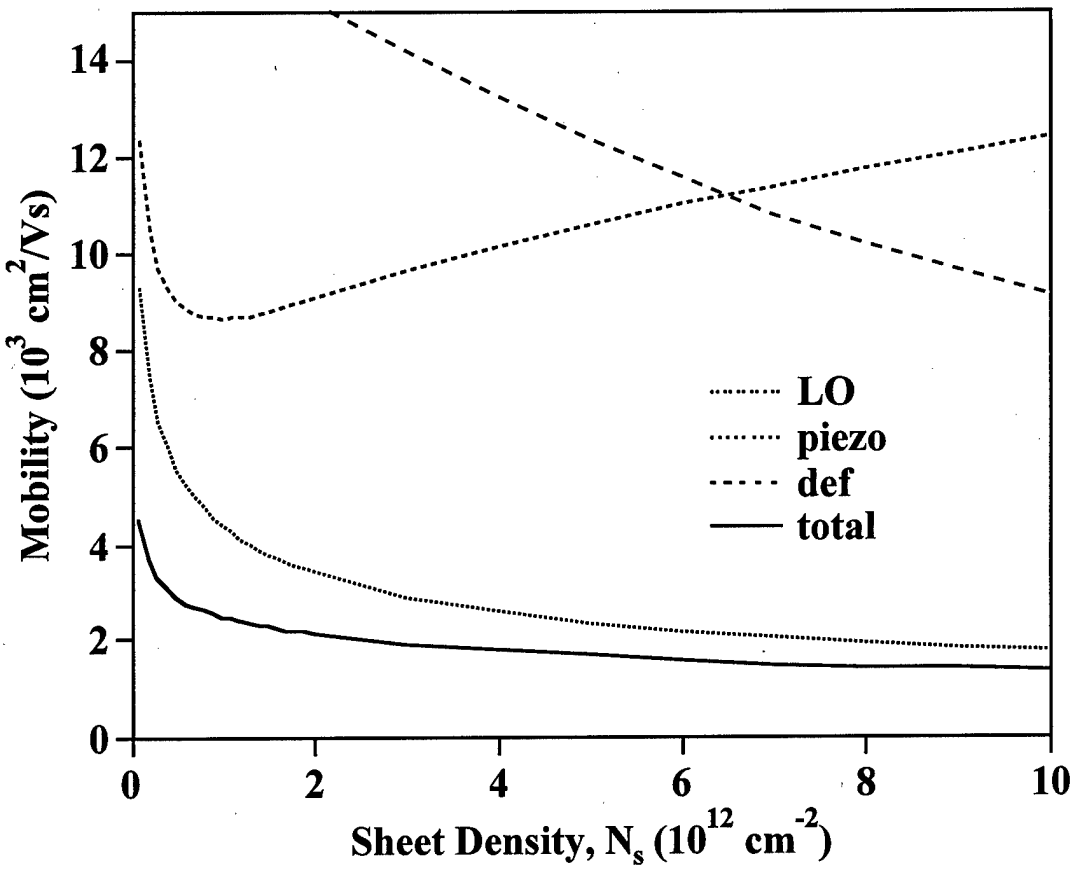

Figure 4: The polar optical phonon, piezoelectric, and acoustic deformation potential components of the 2DEG low-field mobility at the AlGaN/GaN interface.

Measurement of 1/f Noise

In cooperation with Prof. Michael Shur the 1/f noise of several of our devices were measured. Preliminary results show a strong correlation between 1/f noise and device performance including the DC current slump. Analysis of this data is continuing.

References

[1] B.E. Foutz, S.K. O'Leary, M.S. Shur, and L.F. Eastman, "Transient Electron Transport in Wurtzite GaN, InN, and AlN," *J. Appl. Phys.* **85**, 7727 (1999).

[2] B.E. Foutz, M.J. Murphy, O. Ambacher, V. Tilak, J.A. Smart, J.R. Shealy, W.J. Schaff, and L.F. Eastman, "The Influence of SPontaneous and Piezoelectric Polarization on Novel AlGaN/GaN/InGaN Device Structures," *Materials Research Society Symposium Proceedings*, Spring 1999, to be published.

[3] B.E. Foutz, O. Ambacher, M.J. Murphy, V. Tilak, and L.F. Eastman, "Polarization Induced Charge at Heterojunctions of the III-V Nitrides and their Alloys, " The Third

International Conference on Nitride Semiconductors, accepted for the proceedings to be published in Physica Status Solidi.

[4] B. Foutz, "Industry Shows Support for Wide Bandgap Semiconductors at the Spring MRS Meeting," *Compound Semiconductor* **5**, 21 (June 1999).

[5] B.K. Ridley, B.E. Foutz, and L.F. Eastman, "Mobility of 2D Electrons in an AlGaN/GaN Heterostructure," submitted to Phys, Rev. B.

C. Theoretical Study and Modeling of Group III-Nitride Devices – M. Shur

During the last year, our work has concentrated in several areas:

1. Studies of pyroelectric and piezoelectric effects in GaN-based devices
2. Studies of transport properties of GaN-based materials
3. 1/f noise studies of GaN materials and AlGaN/GaN HEMTs
4. Design of novel devices

Studies of piezoelectric and pyroelectric effects
We reviewed pyroelectric and piezoelectric properties of GaN-based materials. We explored using piezoelectric and pyroelectric effects in heterostructures for a drastic reduction of the base spreading resistance in GaN-based Heterostructure Bipolar Transistors. We also studied pyroelectric effect in AlN and showed that AlN is a viable pyroelectric material.

Studies of transport properties of GaN-based materials
We collaborated with the Cornell group in the studies of Monte Carlo simulation of InGaN and AlGaN transport properties. We developed the theory of high-field transport in 2D electron gas. We studied the effect of piezo doping on electron mobility.

1/f-noise studies of GaN materials and AlGaN/GaN HEMTs
We measured 1/f noise on bulk GaN with a record high mobility and in a large number of HEMT devices. We studied the temperature dependence of noise and extracted parameters of local centers responsible for noise. We found the correlation between the leakage current and noise.

Design of novel devices
We developed a novel GaN-based MOSFET that has a better linearity and a very small leakage current (6 orders of magnitude improvement over the conventional GaN-based HFET).

References

[1] M. S. Shur, A. D. Bykhovski, R. Gaska, Pyroelectric and Piezoelectric Properties of GaN-Based Materials, *MRS Internet J. Nitride Semicond. Res.* ***4S1***, G1.6 (1999)

[2] B. E. Foutz, S. K. O'Leary, M. S. Shur, and L. F. Eastman, Transient Electron Transport in Gallium Nitride, Indium Nitride, and Aluminum Nitride, J. Appl. Phys., Vol. 85, Issue 11, pp. 7727-7734, June 1 (1999)

[3] M. E. Levinshtein and S. L. Rumyantsev, D. Look, R. J. Molnar, M. Asif Khan, G. Simin, V. Adivarahan, and M. S. Shur, Low frequency noise in n-GaN with high electron mobility. Journal of Applied Physics, accepted for publication

[4] M. S. Shur and M. Asif Khan, GaN and AlGaN Devices: Field Effect Transistors and Ultraviolet Photodetectors, Academic Press, Semiconductors and Semimetals, S. Pearton, Editor (1999), to be published

[5] S. Jursenas, G. Kirilcik, G. Tamulaitis, A. Zukauskas, R. Gaska, M. S. Shur, M. A. Khan, and J. W. Yang, Dynamic behavior of Hot Electron-Hole Plasma in Highly Photoexcited GaN Epilayers, Appl. Phys. Lett. accepted

[6] W. Knap, E. Frayssinet, M. L. Sadowski, C. Skierbiszewski, D. Maude, V. Falko, M. Asif Khan, and M. S. Shur, Effective g* factor of two dimensional electrons in GaN/AlGaN heterojunctions, Appl. Phys. Lett. accepted

[7] Alexander Dmitriev, Valentin Kachorovskii, Michael S. Shur, and Michael Stroscio, Electron Drift Velocity of Two Dimensional Electron Gas in Compound Semiconductors, International Journal of High Speed Electronics and Systems, accepted

IV. MATERIALS

A. Summary – Lester F. Eastman

Semi-insulating 6H SiC has been developed, using Vanadium doping, and delivered by Northrop Grumman to Cornell during the first three years of this program. That technology has been transferred to Airtron Litton. Presently 4H and 6H semi-insulating material is being purchased from CREE and Sterling Semiconductors, respectively. OMVPE growth of undoped AlGaN/GaN HEMT structures on 2-inch sapphire substrates has continued to mature, reaching ~ 1,600 cm^2/V-s low-field electron mobility, with 2DEG density of $1X10^{13}/cm^2$. The structures have no measurable charge or conduction below the 2DEG, or in the top barrier. Thickness uniformity has improved to ± 7%. Growth of these HEMT layers on SiC continues to advance, although measurable density values of deep donors occurs in the top barrier. As a result, excess gate leakage leads to reduced drain-source breakdown voltage in the range of 25-40 V. Even so, large periphery devices using these wafers have yielded > 4 W/mm. MBE growth has now also

reached 1,600 cm^2/V-s low field mobility for electrons with 2DEG density of $1X10^{13}/cm^2$. These wafers are also grown with ~ 20-25 Å GaN top cap to further protect against degradation resulting from any exposure KOH during processing. Uniformity of thickness is ~ ± 3% over 2" sapphire wafers. Initial transistor power performance has yielded 2.5 W/mm at 35% power-added efficiency at only 15 V drain-source bias for single channel devices. Growth on semi-insulting SiC will be emphasized in the future. The interface between sapphire and the AlN nucleation layer has been studied with high-resolution STEM shaving oxygen extending out into the nitride layer.

B. SiC Semi-Insulating Substrates - Godfrey Augustine

In support of Cornell's Multidisciplinary Research Initiative Proposal to develop high power microwave transistors based on GaN and related compounds, the Northrop Grumman Science & Technology Center has been providing conductive and semi-insulating SiC substrates for the development of high quality GaN/AlGaN epitaxial structures at Cornell University. Since the beginning of this program fourteen SiC crystals have been grown most of which resulted in semi-insulating material. From these growths total substrate area delivered to date equals that of 43 wafers of 1.375 inch diameter which includes four semi-insulating 4H-SiC wafers and 28 semi-insulating 6H-SiC wafers. The rest of the wafers delivered were low resistivity n+ and some high resistivity (200 to 2000 Ω-cm) 4H-SiC.

Monocrystalline silicon carbide material is grown by the physical vapor transport (PVT) technique. N^+ crystals are prepared by adding controlled amounts of high purity nitrogen to the inert ambient. Semi-insulating SiC material is produced by intentionally doping with vanadium, which introduces a deep-donor state lying near the middle of the band gap and compensate the acceptors due to residual boron. A significant increase in the resistivity of these vanadium-doped crystals is observed. However, the addition of the proper amount of vanadium is essential in obtaining high quality semi-insulating SiC material. The amount of vanadium added should be just enough to compensate the residual boron. If too little vanadium is added, all the residual boron is not compensated and the material remains p-type conducting. If too much vanadium is added, the excess vanadium precipitates as vanadium-carbide or vanadium-silicide and results in high defect density. Since the beginning of this program we have obtained a good understanding of the amount of vanadium that should be added to obtain high quality semi-insulating material which has significantly increased the yield of our semi-insulating material and reduced the cost of semi-insulating wafers. Recently, all SiC wafers delivered have been semi-insulting 6H-SiC for the growth of epitaxial GaN layers. The surface normals of these wafers were along the <0001> c-axis direction. The total of sixteen semi-insulating 6H-SiC wafers have been delivered this year.

C. Flow Modulation Epitaxy of AlGaN/GaN HEMT Structures by OMVPE
J.A. Smart and J.R. Shealy

Progress:

Over the past year, substantial advances were made in the OMVPE growth of undoped AlGaN/GaN HEMT structures on both sapphire and semi-insulating SiC substrates. A better understanding of not only crystal growth parameters, but also material properties has led to improvements within the transistor structure. The role of abundant threading dislocations on full channel currents and RF dispersion for undoped HEMT structures is being defined and modeled, explaining the lower than predicted 2DEG densities for a given Al content in the barrier. Using our single temperature growth process with an AlGaN nucleation layer, we achieved reasonable compositional and thickness uniformity across 2-inch substrates. Figure 1 shows a GaN thickness contour plot over a sapphire substrate, with the center 85% very uniform providing sufficient area for circuit fabrication. By design, our reaction cell is able to simultaneously accommodate up to eight 2-inch wafers per process run, producing large areas of uniform epitaxial material. The nucleation layer required optimization on each substrate type to insure insulating GaN buffers and high 2DEG mobilities at the top AlGaN/GaN heterostructure[1]. Growth emphasis is now focused on optimization of the 2DEG mobility and AlGaN barrier thickness uniformity across 2-inch sapphire and SiC substrates.

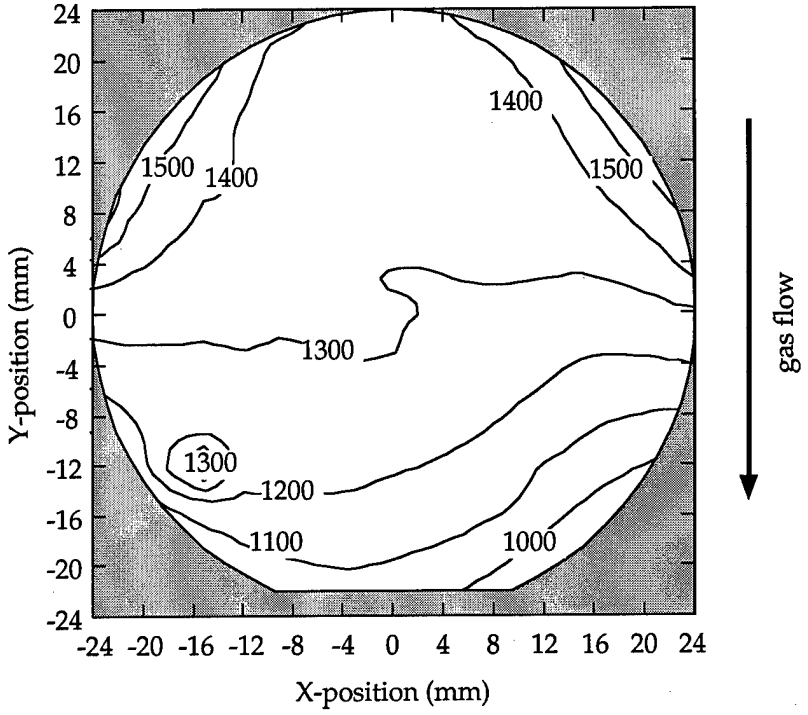

Figure 1. GaN layer thickness uniformity over an entire 2 inch sapphire substrate. Thickness numbers are in nanometers.

To improve transport properties of the 2DEG, the GaN buffer layer thickness was increased from the standard 1 μm to 3 μm. The 1 μm buffer results in planar growth with bi-layer steps observed in AFM analysis, but has large circular features uniformly distributed over the surface as seen in Figure 2 (a). This is a long range roughening of the surface, which does not appear to effect device performance. By increasing the buffer

thickness to 3 μm, the circular features merge together resulting in a smoother growth surface as seen in Figure 2 (b). Room temperature 2D electron mobilities increased from 1465 cm^2/Vs (1 μm) to 1585 cm^2/Vs (3 μm) on samples with nominally $1x10^{13}$ cm^{-2} 2DEG density, indicating a significant improvement in interface roughness at the AlGaN/GaN heterostructure.[2]

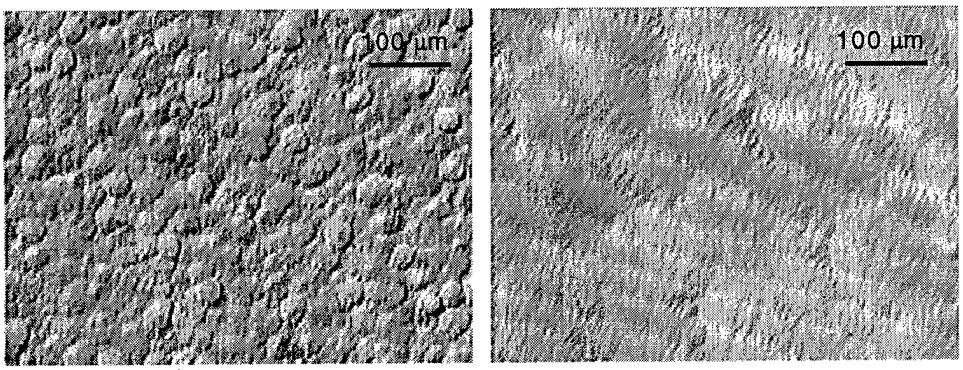

(b) (a)

Figure 2. Nomarski micrographs of surface morphology of AlGaN/GaN transistor structures grown on sapphire substrates. Figure (a) has a 1 μm GaN buffer which shows "puck-like" surface features, while (b) employs a 3 μm GaN buffer resulting in a smoother surface.

Initial growth experiments on SI-SiC focused on optimization of the nucleation layer for producing planar films with low background carrier concentrations. Figure 3 shows surface morphology images of the transistor structure on various SI-SiC substrates from one growth run. Image 1A is from a 2 inch substrate while 1B is from a 1-3/8 inch substrate from the same vendor. Voids are clearly seen on 1B, aligned along straight lines corresponding to surface scratches on the substrate. We can eliminate these voids by either increasing the Aluminum content, or the thickness of the nucleation layer. However, both these corrective measures can lead to other problems within the device structure, such as introducing free carriers in the GaN buffer creating shunt RF conduction paths in the nucleation layer or cracking of the epitaxial layer upon cooling. Therefore, a narrow process window must be defined for each substrate "group" in which the Aluminum content and thickness of the nucleation layer are minimized while still producing device quality epitaxy. The images on the right (2A&B) are structures deposited on 1-3/8 inch SI-SiC from a second vendor. The top right micrograph shows voids similar to those in 1B, which can be eliminated as discussed above. In 2B, circular features are seen on the entire surface with some indications that they follow scratches on the substrate surface. From past experience, the substrate in 2B was "over nucleated", suggesting that the Aluminum content was too high in the nucleation layer for that particular surface finish.

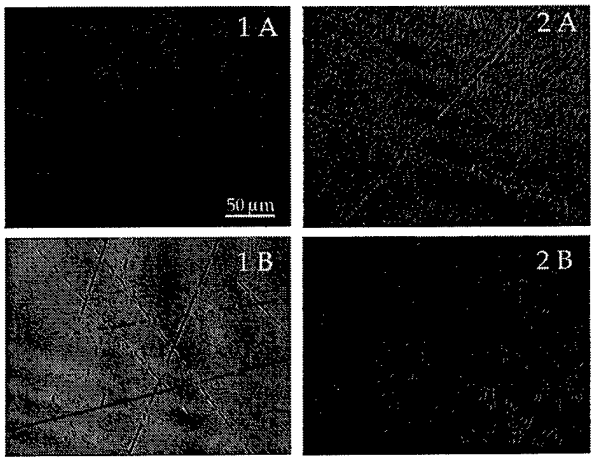

Figure 3. Nomarski surface images of transistor structure deposited on various Semi-Insulating SiC substrates. These 4 substrates were all in the same epitaxial growth run.

Finally, thickness uniformity of the thin AlGaN barrier (along the gas flow direction) was improved by slightly decreasing the growth temperature. At our deposition temperature, we are very close to the Ga desorption limit, and small temperature fluctuations can significantly effect the (Al)GaN growth rate. Since the barrier is on the order of several hundred Angstroms, a subtle temperature gradient (near the desorption limit) across the wafer can cause large variations in film thickness. By lowering the growth temperature from 1040 °C to 1025 ° C, we have improved the AlGaN thickness uniformity from ± 23 % to less than ± 7 % as shown in Figure 4. Initial results on 2-inch SI-SiC is also presented in Figure 4, giving a ± 11 % variation in barrier thickness. It is expected that with additional experimentation, we can improve the AlGaN barrier thickness uniformity to ± 5 %.

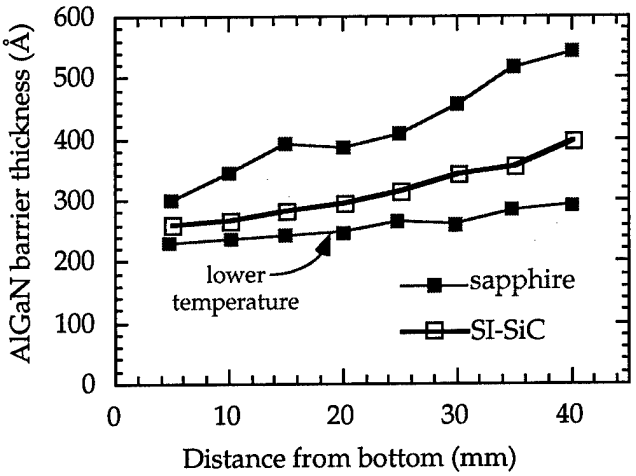

Figure 4. AlGaN barrier layer uniformity in the gas flow direction on HEMT structures on sapphire and SI-SiC substrates.

OMVPE growth for this next year will focus mainly on deposition of undoped AlGaN/GaN HEMTS on SI-SiC substrates. We will continue to investigate layer thickness and compositional uniformity issues on full wafers. This will provide large uniform areas of HEMT material required for monolithic circuit fabrication by other program members. Efforts will also be directed on making our nucleation technology less sensitive to SI-SiC surface finishes. This will involve extensive contact with substrate manufacturers and evaluations of various SI-SiC substrates.

1 J.A. Smart, A.T. Schremer, N.G. Weimann, O. Ambacher, and J.R. Shealy, Appl. Phys. Lett.**75**, (1999).

2 O. Ambacher, J. Smart, J.R. Shealy, N.G. Weimann, M. Murphy, W.J. Schaff, L.F. Eastman, R. Dimitrov, L. Wittmer, M. Stutzmann, Walter Rieger and J. Hilsenbeck, J. Appl. Phys. **85**, (1999)

D. MBE Growth of GaN HEMT's – William Schaff

The past year of effort has resulted in MBE grown GaN HEMT's with small signal and large signal RF characteristics that are state-of-the-art for the dimensions and frequencies studied. At this point last year, there were no DC or RF results; only Hall and CV measurements of 2DEGs. There remain significant challenges to routine MBE growth of GaN HEMT's. The initiation of Ga-face growth on sapphire and SiC is still not a reproducible process. The major impediments to reproducibility have been addressed through DURIP proposals for equipment which is expected to eliminate these problems.

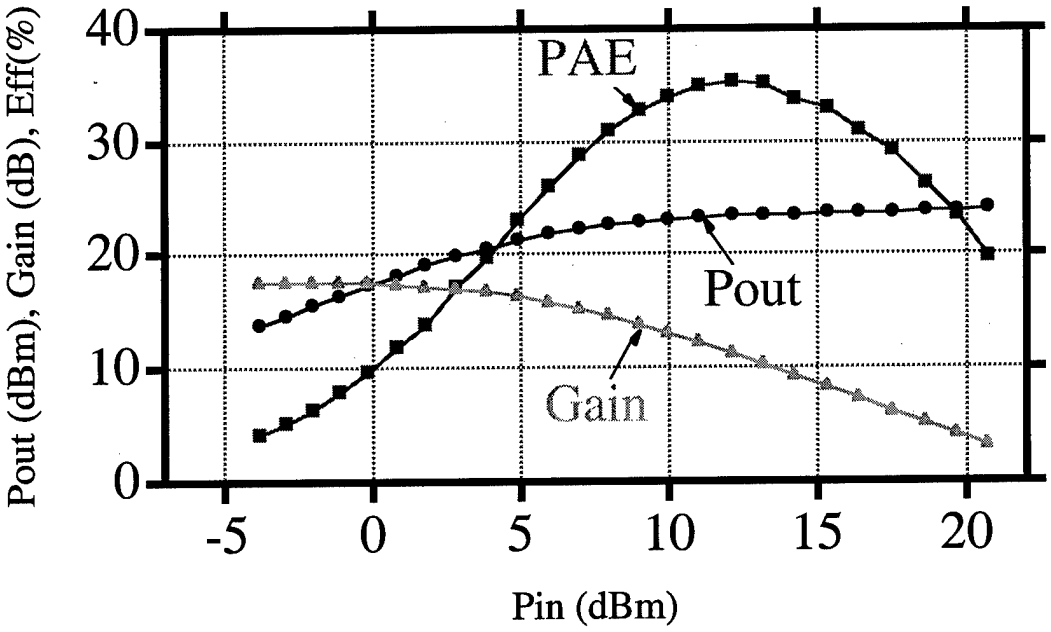

Figure 1. Large signal characteristics of MBE grown GaN 0.4x100 μm HFET 2.50 W/mm at 4GHz_35% PAE max, V_{ds}=15V, I_{ds}=67mA, Vgs=-3.5V

Large signal 4 GHz characteristics for a MBE grown HEMT on sapphire are seen in figure 1. The output power is quite high for this relatively low drain bias voltage. Noise measurements will be conducted on this group of HEMT's. Higher bias voltage measurements will be performed at the Naval Research Laboratory. The processed wafer was sent there in August.

Uniformity for MBE grown HEMT's has been measured by ellipsometry. The GaN thickness as a function of radial position is shown in figure 2. There is a very slight asymmetry which would not normally be expected for MBE growth. A possible explanation comes from the substrate mount geometry. The springs which are supposed to hold the substrate mount at a fixed angle to the furnaces, or substrate heater. These springs lose their tension at the substrate temperatures used for growing GaN and cause

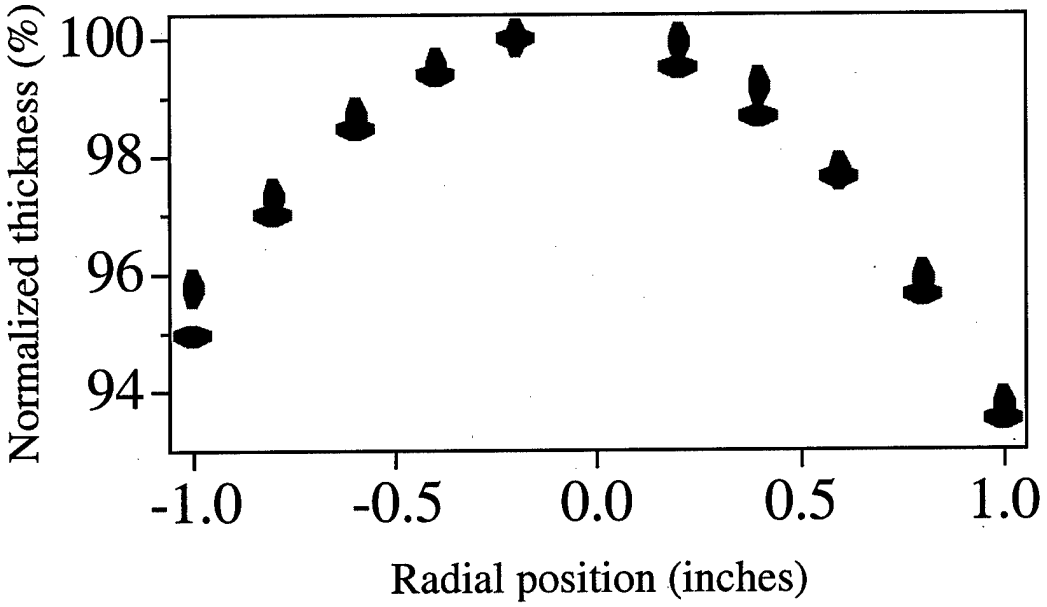

the mount to become tilted.

Figure 2. Uniformity of GaN thickness for a GaN HEMT grown on sapphire by MBE.

E. Nitride characterization by UHV-STEM - Tyler Eustis and Prof. John Silcox

I. Experimental

The HEMT structure used in this study were grown by MBE. The substrate at ~930 °C was initially exposed to a 500 W nitrogen plasma for three minutes. The AlN nucleation layer was deposited at 800 °C at a rate of about 0.32 μm/hr. The nucleation layer was followed by a thick GaN buffer layer grown at the same temperature with no growth interruption. The barrier was comprised of 250 Å of nominally Al_2Ga_8N deposited at 850

°C. The barrier was capped with nominally 30 Å of GaN. The structure contains no intentional doping. Hall mobilities of 1238 cm^2/V-sec and 3182 cm^2/V-sec were obtained at 300 K and 77K, respectively.

The sample was prepared by standard tripod polishing techniques to form a wedge specimen. The sample was ion milled for final thinning.

Parallel Electron Energy Loss Spectrums (PEELS) of the nitrogen and oxygen K-edges (atomic 1s to conduction band) were taken simultaneously and individually, stepping across the GaN/AlN/Sapphire interfaces. PEELS of the aluminum L_{23}-edge (atomic 2p to conduction band) were also collected stepping across the interfaces. ADF images of the interface taken immediately before and after acquisition of the spectrums indicate an insignificant spatial drift.

All data and images are acquired digitally. After acquisition, the spectrums were smoothed and shot noise was removed. The background was subtracted using a standard power-law curve fit to the pre-edge. The intensities of the nitrogen and oxygen core edges were integrated over 50 eV starting at threshold. Ratios of O/N+O were obtained

$$\frac{N_A}{N_A+N_B}=\frac{I_A(\beta,\Delta)}{I_A(\beta,\Delta)+\left(\sigma_A/\sigma_B\right)I_B(\beta,\Delta)} \qquad \text{Equation 1}$$

using the standard equation involving integrated intensities and cross

where $\sigma_K(\beta,\Delta)$ is the partial cross section for the inner shell excitation of element K over the energy range Δ and for scattering angles up to β; $I_K(\beta,\Delta)$ is the integrated intensity of the edge within the energy range Δ and for scattering angles up to β.

Serin et. al. reported observing electron beam induced damage in similar material (AlON). Based on their results acquisition times on the order of 0.5 sec. were used, in an attempt to avoid damage. This prevented damage in the nominally AlN layer. However, damage was observed in the sapphire by the characteristic high intensity of the first nitrogen peak. In fact, upon stepping across the AlN/sapphire interface, it was possible to "drag" nitrogen into the sapphire bulk. Acquisition times on the order of 0.1 sec. were required to prevent damage ("dragging" nitrogen into the sapphire). Such short time caused a low signal to noise ratio. In Figure 1 are two nitrogen K-edges. A high peak is seen deep within the sapphire for the longer acquisition time indicating damage. No nitrogen signal was observed for the shorter time. Thus as a compromise, the data taken with an acquisition time of 0.5 sec. will be used with the knowledge that the nitrogen signal within the sapphire is damage induced.

II. Results

An ADF image of the GaN/AlN/sapphire interfaces is presented in Figure 2(a). The line marks where the data points in Figure 2(b) and (c) were collected. Again, the edges were integrated from threshold to 50 eV above threshold. The integrated intensities are plotted

in Figure 2(b). The drop in nitrogen signal going into the GaN is due to a decrease in thickness determined from low loss data. Figure 2(c) depicts the ratio O/O+N based on the data in 2(b). The ratio data was fit with two sets of two exponentials. A vertical line is drawn at the intersection of each set representing the possible interface between the AlN and sapphire.

A TEM Bright Field image of the AlN/sapphire interface is presented in Figure 3.

III. Discussions

The presence of aluminum oxynitride at the III-N/sapphire interface has been under debate. Uchida et. al. reported on the formation of an amorphous aluminum oxynitride upon nitridation of the sapphire substrate by NH_3 in an MOVPE apparatus. However, others have reported that upon nitridation of sapphire by NH_3, the surface undergoes complete conversion to AlN before subsequent layers are converted. Complete conversion also occurs upon nitridation by the Oxford Car25 plasma source in an MBE system. It has also been reported that nitridation of sapphire using the EPI Uni-Bulb plasma source can produce an aluminum oxynitride. However, to date, no report has been made on the oxidation of AlN buffer layers by the sapphire substrate, which we report here.

The presence of oxygen is observed in the nominally AlN buffer layer upon examination of Figure 2. From Fig. 2(b), the oxygen signal is constant in the sapphire. At the AlN/sapphire interface, based on the ADF image in Fig. 2(a), the oxygen signal drops sharply, subsequently tailing off into the AlN. Remember, as stated above, the nitrogen signal within the sapphire is radiation induced, hence the ratio depicted in Fig. 2(c) does not level off in the sapphire at one. The ratio begins to decrease as the oxygen signal decreases and the nitrogen signal increases across the AlN/sapphire interface. Once across the interface, the oxygen signal decays and reaches zero at the AlN/GAN interface. It is unclear why the oxygen signal reaches zero at the AlN/GaN interface. One possibility is that it is just a coincidence. Another is the oxygen does not have the same driving force to diffuse into the GaN as it does with AlN. The driving force could be chemically and/or structurally related. Studies of oxygen diffuison into AlN from Al_2O_3 suggest that no significant diffusion should occur at the temperatures used during growth. Another possible driving force could be the strain due to the lattice mismatch between the AlN and sapphire. However, here the strain would actually prevent diffusion. A third possibility is that the formation of an intermediate phase, AlON, could drive the diffusion of oxygen into the AlN. Comparing Figure 3 with Figure 2, it appears there is an intermediate phase of AlON which might be structurally different from the AlN and sapphire. However, the diffraction pattern only shows spots corresponding to AlN and sapphire. An intermediate AlON phase could lower the total energy of the system through either chemical or structural avenues.

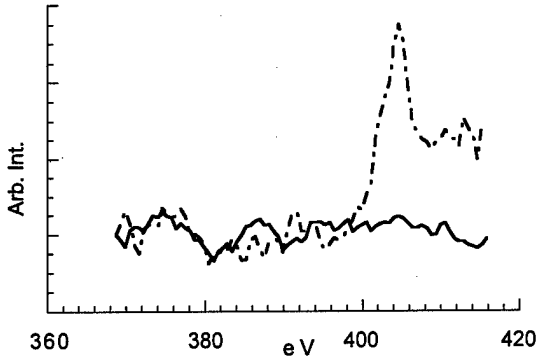

Figure 1. Nitrogen K-edge in sapphire with an without beam induced damage.

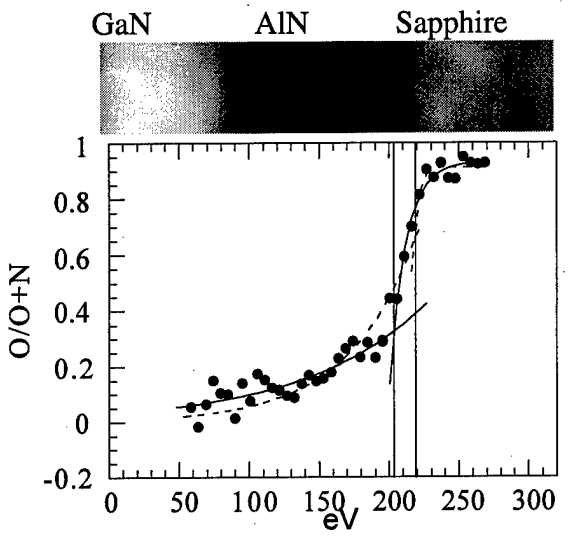

Figure 2(a) and (b)

(a)ADF image of GaN/AlN/sapphire interface

C. O/O+N

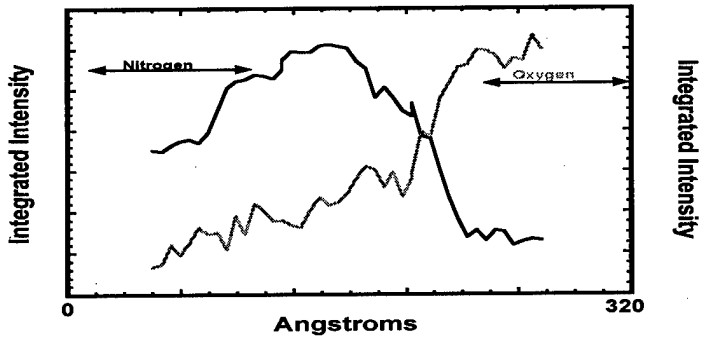

Figure 2(b). EELS Integrated Intensity for Oxygen and Nitrogen

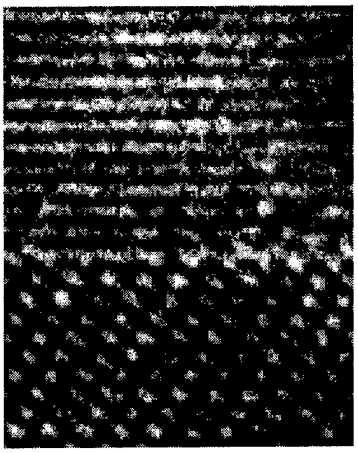

Figure 3. AlN/sapphire interface. Sapphire is at the bottom.